Quantification of Retinal Oxygen Extraction Fraction

and Vascular Oxygen Tension Gradients

BY

PANG-YU TENG

BS, Chung Yuan Christian University, 2005
MS, University of Illinois at Chicago, 2009

THESIS

Submitted as partial fulfillment of the requirements
for the degree of Doctor of Philosophy in Bioengineering
in the Graduate College of the
University of Illinois at Chicago, 2014

Chicago, Illinois

Defense Committee:

Mahnaz Shahidi, Chair and Advisor, Ophthalmology & Visual Sciences
Norman P Blair, Ophthalmology & Visual Sciences
Jun Cheng
John R Hetling
Thomas Royston

ACKNOWLEDGMENTS

I would like to thank my thesis committee--(*Mahnaz Shahidi, Norman P Blair, Jun Cheng, John R Hetling, and Thomas Royston*)--for their unwavering support and assistance. They provided guidance in many areas that helped me accomplish my research goals and learn the process of research. I would also like to thank the staffs at the Illinois Eye and Ear Infirmary, University of Illinois College of Medicine at Chicago, in particular, Marek Mori, Tara Nguyen, Justin Wanek, Ruth Zelkha for their guidance and help in the data collection process. Lastly, I thank my friends and family for their constant support.

CONTRIBUTION OF AUTHORS

Chapter I states the motivation and significance of my research in this dissertation in the context of a larger field, oxygen measurements in the retina. Chapter II is a literature review on the field of my research. Chapter III and VI represent unpublished data from experiments which validated my proposed methods for semi-automated quantification of oxygen levels in 2D and 3D phosphorescence images, respectively. Chapter V represents a published manuscript, “Inner Retinal Oxygen Extraction Fraction in Rat“,(Teng, et al. 2013) for which I was the first author and was involved in the planning and execution of experiments, data analysis and writing of the manuscript. Justin Wanek contributed to the planning and execution of the experiments, and writing of the manuscript. Norman Blair and Mahnaz Shahidi contributed to the planning of the experiments and writing of the manuscript. Chapter VI represents unpublished work that investigated the response of inner retinal oxygen extraction fraction to light flicker. Chapter VII represents a published manuscript, “Oxygen Tension and Gradient Measurements in the Retinal Microvasculature of Rats”,(Teng, et al. 2012) for which I was the first author and was involved in the planning and execution of experiments, data analysis and writing of the manuscript. Justin Wanek contributed to the execution of the experiments and writing of the manuscript. Norman Blair and Mahnaz Shahidi contributed to the planning of the experiments and writing of the manuscript.

TABLE OF CONTENTS

LIST OF TABLES

LIST OF FIGURES

LIST OF FIGURES (continued)

LIST OF ABBREVIATIONS

2D	Two Dimensional
3D	Three Dimensional
gPO_2	Oxygen Tension Longitudinal Gradient
OEF	Oxygen Extraction Fraction
PLI	Phosphorescence Lifetime Imaging
PO_2	Oxygen Tension
SO_2	Oxygen Saturation

SUMMARY

Energy metabolism in the retinal tissue of the eye is considered to be one of the highest in the body. In order to maintain this highly metabolic demand for visual processing and vision, a constant delivery of oxygen by the retinal circulation is required. Alterations in retinal circulation due to vascular abnormalities are implicated in many retinal diseases and may lead to abnormal oxygenation of the retinal tissue. As a result, parameters that characterize the retinal oxygenation may help advance our understanding in both healthy and diseased retinas.

This thesis describes novel methods for determining oxygen extraction parameters based on retinal vascular oxygen tension (PO_2) measured by phosphorescence lifetime imaging. First, semi-automated vessel segmentation methods for quantifying the vascular PO_2 from two- (2D) and three-dimensional (3D) phosphorescence lifetime images were developed and validated. Inner retinal oxygen extraction fraction (OEF) and vascular PO_2 longitudinal gradients (gPO_2) of retinal vessels in rats were then derived based on vascular PO_2 from 2D and 3D images, respectively. Measurements of gPO_2 in retinal vessels were validated by determining its response to hypercapnia. Quantification of inner retinal OEF was established and validated by measuring its alteration due to a severe hypoxic challenge. The effect of light flicker stimulation on OEF was also determined, thus demonstrating a method for assessment for neurovascular coupling in terms of the compensatory capacity of blood flow increase in response to increased oxygen metabolism.

Methodologies for measurements of inner retinal OEF and vascular gPO_2, and assessment of neurovascular coupling by OEF were demonstrated for the first time. These methods can serve as useful tools for investigating retinal oxygenation in health and disease.

I. INTRODUCTION

The energy metabolism of the retina is considered to be one of the highest in the body. In order to maintain this highly metabolic demand, a constant delivery of oxygen by the retinal circulation is required. Alterations in retinal circulation due to vascular abnormalities may lead to tissue hypoxia, a condition that impairs neural activity (Linsenmeier 1990) and is implicated in many retinal diseases.(Kur, et al. 2012; Osborne, et al. 2004) Indeed, under a severe hypoxic or ischemic insult, retinal function has been shown to be impaired,(Anderson 1968; Linsenmeier 1990; Osborne, et al. 2004; Weidner 1976), and will become irreversibly damaged if the hypoxia/ischemia is sustained.(Hayreh and Weingeist 1980; Hayreh, et al. 2004; Osborne, et al. 2004) Furthermore, abnormal vascular oxygen levels have been reported in vascular occlusions,(Hardarson, et al. 2013; Jaime, et al. 2012) diabetic retinopathy,(Hardarson and Stefansson 2012; Khoobehi, et al. 2013) glaucoma,(Olafsdottir, et al. 2011; Olafsdottir, et al. 2014) and oxygen-induced retinopathy.(Mezu-Ndubuisi, et al. 2013) As a result, further investigation of oxygen levels in retinal vessels are needed for the advancement of knowledge in retinal physiology and pathological processes.

Current available imaging techniques for quantification of retinal vascular oxygen levels include oximetry,(Hammer, et al. 2008; Hardarson, et al. 2006) and phosphorescence lifetime imaging (PLI).(Shahidi, et al. 2006; Shahidi, et al. 2010; Shahidi, et al. 2009; Shonat and Kight 2003; Wilson, et al. 2005a) Oximetry is an optical method for quantification of the retinal vascular oxygen saturation (SO_2, percent of hemoglobin carrying oxygen) by measuring the vascular optical densities at different wavelength.(Beach, et al. 1999; Delori 1988; Hickam, et al. 1963) The use of oximetry has gained considerable interest in retinal research since it can noninvasively provide information about retinal oxygenation in humans.(Eysteinsson, et al. 2014; Geirsdottir, et

al. 2014; Geirsdottir, et al. 2012; Hardarson, et al. 2013; Hardarson and Stefansson 2012; Jani, et al. 2014; Jorgensen, et al. 2014; Khoobehi, et al. 2013; Olafsdottir, et al. 2014; Traustason, et al. 2014; Vandewalle, et al. 2013) There are however technical limitations in the current oximetry systems. Such limitations include, bright specular reflex of vessels which could adversely affect measurement reliability, and signal contribution from the choroidal vessels which precludes measuring SO_2 in smaller-ordered vessels, such as those branching off from the major retinal vessels.(Hammer, et al. 2001) As a result, reliable SO_2 has only be reported in major retinal vessels (> ~100 μm in width) in humans and pigs.(Delori 1988; Hammer, et al. 2001; Hammer, et al. 2008; Hardarson, et al. 2006; Hickam, et al. 1963; Palsson, et al. 2012; Traustason, et al. 2013)

PLI is an optical method that can measure oxygen tension (PO_2) by obtaining the phosphorescence lifetime of an oxygen-sensitive molecular probe (Pd-porphine). This method has been used to investigate the vascular oxygen dynamics in the retina,(Riva 1998; Shonat and Kight 2003; Wilson, et al. 2005a) and also the microvascular and tissue PO_2 outside the eye.(Intaglietta, et al. 1996; Tsai, et al. 2003) However, similar to retinal oximetry, PO_2 measured in smaller-ordered vessels have also been precluded due to phosphorescence signal contamination from the underlying choroid.(Shonat and Kight 2003; Wilson, et al. 2005a) Overcoming this limitation, Shahidi et al. developed an imaging system that combined PLI with optical sectioning,(Shahidi, et al. 2006) which allowed imaging of cross sectional depth resolved PO_2 of both retinal and choroidal vessels. With this imaging system, reliable vascular PO_2 measurements could be obtained in both major and smaller-ordered retinal vessels. In addition to acquiring vascular PO_2 in 2D, vascular PO_2 can also be obtained in 3D by acquiring contiguous cross sectional images across the retina.(Shahidi, et al. 2009) Imaging of the vascular

PO_2 in 3D opens up the possibility of investigating the oxygen dynamics in the entire complex retinal microvascular network.

With the capability of imaging the retinal vascular PO_2 in 2D and 3D in animals by PLI, the questions then arise as to:

1) How to efficiently quantify the vascular PO_2 in 2D and 3D phosphorescence images?

2) What are the parameters that could be used to gauge the amount of oxygen extraction or the adequacy of oxygen delivered to the retina, both globally and locally?

This thesis attempts to provide solutions to these questions by establishing novel semi-automated methods for quantification of vascular PO_2 in 2D and 3D phosphorescence images and utilizing the semi-automatically quantified PO_2 measurements to derive global and local retinal tissue oxygen extraction parameters. Specifically, a semi-automated vessel lumen method for quantifying retinal vascular PO_2 from 2D PLI was developed and validated by quantifying vascular PO_2 from digital vascular phantom images. Additionally, the repeatability of the method was assessed by comparing the semi-automatically and manually quantified vascular PO_2. The vascular PO_2 quantified by the semi-automated method was demonstrated to have a higher repeatability than when the manual method was used.

Using the semi-automated vessel lumen segmentation method, retinal arterial and venous PO_2 was measured in rats and used to derive inner retinal oxygen extraction fraction (OEF) for the first time.(Teng, et al. 2013) The parameter, OEF, has been demonstrated to be useful for determining ischemia-induced hypoxia in cerebral tissue.(Derdeyn 2007; Powers 2012; Powers and Zazulia 2010), and could be useful in determining similar conditions in the retina. Measurements of OEF were validated by demonstrating an increase in OEF under a severe hypoxia challenge in rats. In addition,

the effect of light flicker on OEF during normoxia and hypoxia was investigated. The rationale for investigating this response was that although both oxygen delivery and metabolism has been shown to increase during increased neural activity, it is uncertain if the increase in oxygen delivery fully compensates for the increase in oxygen metabolism.(Linsenmeier 2012)

The optical sectioning capability of PLI has allowed generation of 3D vascular phosphorescence images. In order to efficiently analyze the vascular PO_2 from these 3D images, a semi-automated vessel tracking method was developed for quantification of the vascular PO_2 along the imaged vessels. This method was validated by quantifying the vascular PO_2 from a 3D digital vascular phantom image. Using the semi-automated method, vascular PO_2 along retinal vessels in rats was quantified and used to determine the vascular PO_2 longitudinal gradients (gPO_2, the PO_2 difference per unit length along vessel segments) in major arteries, veins and microvessels between the arteries and veins.(Teng, et al. 2012) Measurement of gPO_2 was validated by demonstrating an increase during hypercapnia, due to a vasodilatory-induced decrease in oxygen extraction.(Davis, et al. 1998; Kim, et al. 1999; Stefanovic, et al. 2004)

II. BACKGROUND

Retina and Retinal-Choroidal Circulations

The retina is a light-sensitive multi-layered tissue situated in the posterior inner surface of the eye (Fig 1A). As a part of the visual system, the role of the retina is to convert the perceived light to electrical signals. These signals are then transmitted to the cerebral cortex through the optic nerve for further visual processing.(Boron and Boulpaep 2005) To maintain a normally functioning retina, a high level of energy is produced and consumed, thereby requiring a constant supply of oxygen to be delivered to the retina.(Braun, et al. 1995; Hardarson 2013; Kur, et al. 2012; Newman 2013; Wanek, et al. 2011; Wanek, et al. 2013) Without any delivery of oxygen to the retina, the retina will cease to function, leading to loss of vision in less than a minute.(Anderson 1968)

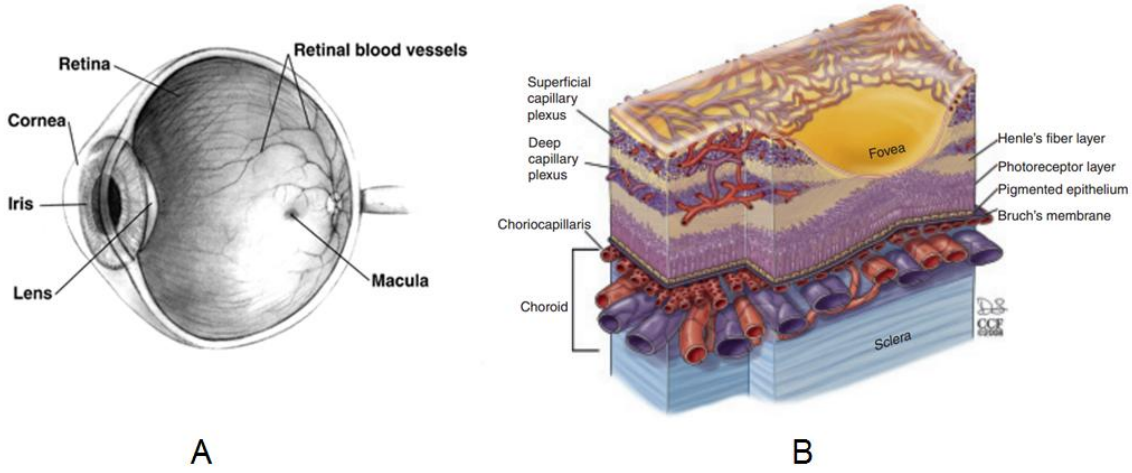

Fig. 1 A) A cross sectional view of the eye displaying the retina in the posterior inner surface of the eye (Figure reprinted from Wikipedia). (National Eye Institute 2014) B) A cross sectional view of the retinal tissue, displaying the retinal and choroidal circulations which are in the anterior half (top) and posterior (bottom) of the retina, respectively (Figure reprinted from Anand-Apte B, et al.). (Anand-Apte 2011)

The oxygen supplied to the retina is delivered from blood through two circulations, the choroidal and retinal circulations.(Hayreh 2011; Kur, et al. 2012; Linsenmeier 2012; Newman 2013) The retinal circulation, situated in and near the surface of the retina (Fig 1B) supplies oxygen to the anterior half of the retina (inner retina). The choroidal circulation, located immediately posterior to the retina (Fig 1b), supplies oxygen through its high highly anastomotic network to the posterior half of the retina (outer retina). The portion of tissue in which each circulation supplies the oxygen varies and is dependent by the relative amount of energy metabolized among the retinal layers. In this thesis, the terms “inner retina” and “outer retina” will be referred to as the portions of tissue in which the oxygen is supplied by the retinal and choroidal circulations, respectively.

Importance of Retinal Oxygenation

Physiological and pathological changes may lead alterations in the delivery and metabolism of oxygen in the retina. These alterations are reflected on the retinal vascular PO_2, SO_2 and retinal tissue PO_2 (the relationships among vascular and tissue oxygen levels and oxygen delivery and metabolism will be explained in section Models of Oxygen Transport). As result, knowledge of retinal vascular and tissue oxygen levels in normal and diseased retinas will lead to better understanding of the retina and the pathophysiology of retinal diseases, respectively. Table I lists some of the findings from past studies that measured either the retinal vascular or tissue oxygen levels under altered physiology or diseased conditions. Since alterations in retinal oxygenation are indications of altered physiology or pathology, measurements of oxygen may be used for assessment of disease progression and even potentially used as biomarkers for early detection of retinal diseases.

TABLE I FINDINGS FROM PREVIOUS STUDIES THAT MEASURED UNCHANGED (↔), INCREASED (↑) OR DECREASED (↓) OXYGEN LEVELS IN EITHER THE RETINAL VESSEL OR TISSUE IN ALTERED PHYSIOLOGY OR DISEASED CONDITIONS IN HUMANS AND ANIMALS.

	Arterial PO_2 or SO_2	Venous PO_2 or SO_2	Inner Retinal Tissue PO_2	Outer Retinal Tissue PO_2
Dark to Light condition	↓ (humans(Hardarson, et al. 2009))	↓ (humans(Hardarson, et al. 2009))	↔ (rats(Lau and Linsenmeier 2012))	↑ (monkeys, cats, (Linsenmeier 2012) rats(Lau and Linsenmeier 2012))
Light Flicker	↔ (humans(Hammer, et al. 2011)), ↑ (rats(Shakoor, et al. 2006))	↑ (humans(Hammer, et al. 2011)), ↔ (rats(Shakoor, et al. 2006))	↓ (rats(Lau and Linsenmeier 2012), cats(Buerk, et al. 1998; Buerk and Riva 2002))	
Severe Hypoxemia			↓ (cats(Linsenmeier and Braun 1992))	↓(cats(Linsenmeier and Braun 1992))
Mild Hypoxemia	↓ (humans(Traustason, et al. 2011))	↓ (humans(Traustason, et al. 2011))	↔ (cats(Linsenmeier and Braun 1992))	↓(cats(Linsenmeier and Braun 1992))
Vascular Occlusion	↓ (human(Hardarson, et al. 2013), rabbits(Jaime, et al. 2012))	↓ (humans(Hardarson, et al. 2013), rabbits(Jaime, et al. 2012))		
Glaucoma	↔ (humans(Olafsdottir, et al. 2011; Olafsdottir, et al. 2014))	↑ (humans(Olafsdottir, et al. 2011; Olafsdottir, et al. 2014))		
Diabetic Retinopathy	↑ (humans(Hardarson and Stefansson 2012; Khoobehi, et al. 2013)), ↔ (humans(Hammer, et al. 2009))	↑ (humans (Hammer, et al. 2009; Hardarson and Stefansson 2012; Khoobehi, et al. 2013))	↓ (cats(Linsenmeier, et al. 1998))	
Oxygen-induced Retinopathy	↔ (mice(Mezu-Ndubuisi, et al. 2013))	↓ (mice(Mezu-Ndubuisi, et al. 2013))		

Theory of Oxygen Transport

The amount of oxygen being delivered by the retinal circulation and consumed by the retinal tissue can be expressed using Krogh's model.(Tsai, et al. 2003) The Krogh's

model applies the principle of mass balance to the transport of oxygen from a blood vessel segment to the tissue that surrounds this blood vessel segment. As oxygenated blood passes through this vessel segment, the PO_2 will be lower in the downstream location as compared to that in the upstream location. This difference in PO_2 is due to an oxygen flux at the vascular wall where oxygen is diffusing outward from the vessel to the tissue. The existence of this oxygen flux is driven by a pressure difference between the intravascular and tissue PO_2, where the tissue PO_2 is lower due to consumption of oxygen by the tissue. Simultaneously, due to this consumption of oxygen, the tissue PO_2 at locations further away from the vessel will also be lower than that near the vessel. The above relationship can be expressed as,

$$Q*(O_{2c\_in} - O_{2c\_out}) = 2*\pi*R_0*L*D*\alpha*(dPO_2/dr) = M*\pi*(R_t^2-R_0^2)*L \qquad (eq\ 1)$$

, where Q is the flow rate of blood, O_{2c_in} and O_{2c_out} are the oxygen contents at the inlet and outlet of the vessel segment, respectively. R_0 is the radius of the vessel segment, L is the length of the vessel segment, D is the diffusion constant, α is the oxygen solubility, and dPO_2/dr is the radial PO_2 gradient at the blood-tissue interface. M is the rate of oxygen consumed by the tissue per unit volume, and R_t is the radius of the tissue surrounding the vessel segment. The vascular oxygen content is the amount of oxygen carried by the hemoglobin and dissolved in blood, and can be obtained by the following equation, (Crystal 2001)

$$O_{2c} = O_{2max} * Hgb * SO_2 + k * PO_2 \qquad (eq\ 2)$$

where O_{2max} is the maximum oxygen carrying capacity of hemoglobin, Hgb is the measured hemoglobin concentration of arterial blood and k is the oxygen solubility in blood (0.003 $mLO_2 \cdot dL^{-1} \cdot mmHg^{-1}$),(Crystal 2001). The vascular SO_2 is dependent mainly on the vascular PO_2, by the oxygen dissociation curve as follows,

$$SO_2 = (PO_2/P_{50})^n/[1+ (PO_2/P_{50})^n] \qquad (eq\ 3)$$

where n is an empirical constant, which varies between species,(Cartheuser 1993) and P_{50} (in mmHg) is the PO_2 when SO_2 is 0.5 at a given pH,(Chen, et al. 2010)

$$\log_{10} P_{50} = \log_{10} (26.4) - 0.48 (pH - 7.4) \qquad (eq\ 4)$$

As an alternative to the Krogh's model, the oxygen transport in the retina can be expressed in an abstract model using Fick's principle (Pittman 2011) by assuming the retina as a block of tissue and the blood in this tissue is being supplied and drained by a single artery and a single vein, respectively. The oxygen delivery (DO_2) and oxygen metabolism (MO_2) of the retina can then be determined as follows,

$$MO_2 = Q * (O_{2A} - O_{2V}) \qquad (eq\ 5)$$

$$DO_2 = Q * O_{2A} \qquad (eq\ 6)$$

, where Q is the flow rate of blood, and O_{2A} and O_{2V} are the oxygen contents in the artery and vein, respectively. Finally, the MO_2 can then be related to DO_2 by OEF with the following equation,

$$MO_2 = DO_2 * OEF = DO_2 * (O_{2A}-O_{2V}) / O_{2A} \qquad (eq\ 7)$$

As shown by equation 7, OEF is the fractional amount of oxygen removed from arterial blood by the tissue.

Methods for Measuring Oxygen Levels in the Vessels and Tissue

The importance of oxygen transport has led to the development of several methods for measuring oxygen levels in the retinal vessels and tissue. The methods discussed here are oxygen-sensitive microelectrodes (Braun, et al. 1995; Buerk, et al. 1993; Lau and Linsenmeier 2012; Linsenmeier 2012; Linsenmeier and Braun 1992; Yu and Cringle 2001; Yu, et al. 1994; Yu, et al. 2007), oximetry (Beach, et al. 1999; Beach, et al. 2007; Hammer, et al. 2001; Hammer, et al. 2008; Hardarson 2013; Hardarson, et al. 2006), and PLI.(Shahidi, et al. 2006; Shahidi, et al. 2009; Shonat and Kight 2003; Wilson, et al. 2005a) These methods either measure the PO_2 in the vessels or tissue, or

SO_2 in the vessels. Other methods for gauging the retinal tissue oxygen level include magnetic resonance imaging (Ito and Berkowitz 2001) and hypoxyprobe (pimonidazole), which is an ex vivo method.(Wright, et al. 2012) Both magnetic resonance imaging and hypoxyprobe cannot determine absolute levels of PO_2 or SO_2 and will not be further discussed in this chapter. Emphasis will be made on PLI, as PLI is the method used for studying the vascular PO_2 in this thesis.

Oxygen-sensitive Microelectrode

The oxygen-sensitive mircoelectrode, also termed the Clark electrode or polargraphy, is considered to be the gold standard and the oldest method for measuring oxygen levels in the retina.(Takahashi, et al. 1966) It can measure the tissue PO_2, and estimate the retinal vascular PO_2 by introducing the electrode to the retina or on the vessel surface, respectively. The oxygen-sensitive microelectrode operates by polarizing a noble metal, such as platinum, at -0.7 volt with respect to a reference electrode.(Linsenmeier 2012) The noble metal then becomes a cathode, where nearby oxygen is chemically reduced. Simultaneously, a current is produced and is recorded to be used for determination of PO_2 at the measured location. The chemical net reaction is as follows: $O_2 + 4e^- + 2H_2O \rightarrow 4OH^-$. Usually, calibrations are performed before and after each experiment by measuring the current from the electrode in several mediums with known PO_2 levels.(Braun, et al. 1992; Padnick, et al. 1999; Tsai, et al. 2003) Assuming a linear relationship between the current and PO_2, these values measured during the calibration are then used to determine the PO_2 from the measured current during the experiment. The microelectrode can only measure one location at a time, thus limiting its spatial resolution. However, there are several advantages for using the microelectrodes, such as its high temporal (50ms(Linsenmeier 2012)) and depth

(3um(Lau and Linsenmeier 2012)) resolutions, and that retinal PO_2 can be measure in both light and dark conditions.

Oximetry

The oximetry, also termed spectrophotometry, measures the retinal vascular SO_2. This method determines the SO_2 by utilizing the varying optical density (OD) of the oxygenated (HbO_2) and deoxygenated hemoglobin (Hb) at different wavelengths.(Beach, et al. 1999; Delori 1988; Hickam, et al. 1963) The ODs of the HbO_2 and Hb over a range of wavelengths,(Van Assendelft 1970; Zijlstra, et al. 1991) in terms of extinction coefficients are shown in Fig 2. The OD is dependent by the amount of oxygen carried by the hemoglobin at most wavelengths (non-isosbestic wavelengths), indicating the amount of light absorbed by blood will be dependent by SO_2. However, in several wavelengths (isosbestic wavelengths), the ODs for both HbO_2 and Hb will be the same, indicating the amount of light absorbed by blood will be independent from SO_2. In theory, the SO_2 of blood can be estimated by quantifying the OD at a non-isosbestic wavelength by assuming a linear relationship between SO_2 and OD.(Van Assendelft 1970) However, in the living tissue, there are multiple factors that affects the measurements of vascular OD, such as absorption and scattering of light by the tissue.(Hammer, et al. 2002) To overcome these factors, current oximetry systems uses vascular ODs from images acquired at multiple wavelengths, usually at least one images at a non-isosbestic wavelength, and one image at an isosbestic wavelength.(Hammer, et al. 2008; Hardarson, et al. 2006; Khoobehi, et al. 2013; Yi, et al. 2013) While oximetry is still under development and is used only in non-clinical settings, it has been validated in pigs (Traustason, et al. 2013) and used extensively to measure retinal vascular SO_2 in humans.(Delori 1988; Hammer, et al. 2001; Hammer, et al. 2008; Hardarson, et al. 2013; Hardarson, et al. 2006; Hardarson and Stefansson 2012; Hickam, et al. 1963; Jaime, et

al. 2012; Khoobehi, et al. 2013; Olafsdottir, et al. 2011; Olafsdottir, et al. 2014; Palsson, et al. 2012) Given that it is a non-invasive imaging method, it holds promise for becoming a clinically approved system for assessing retinal vascular oxygenation.

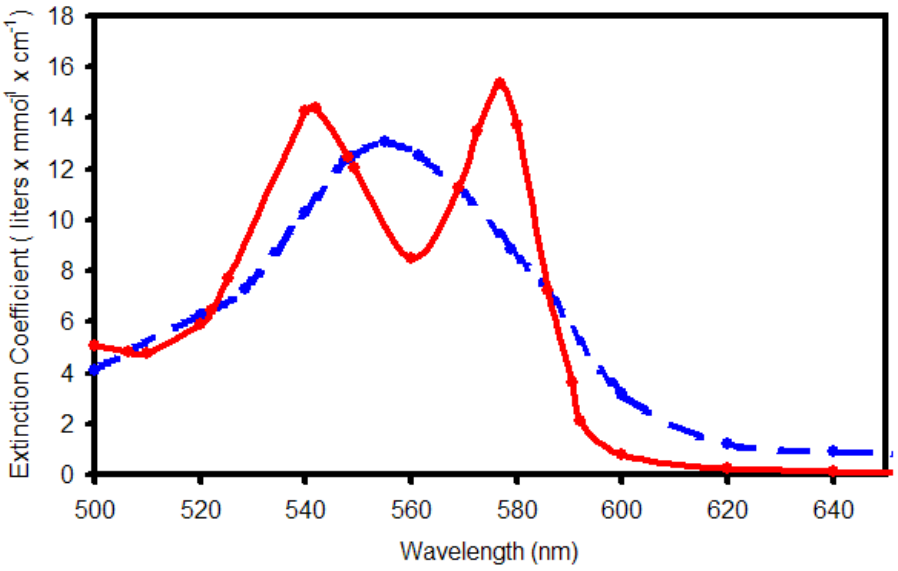

Fig. 2 The absorptivity of the HbO2 (solid line) and Hb (dashed line) over a range of wavelengths, expressed in terms of extinction coefficient. Data extracted from a previous study.(Van Assendelft 1970)

Phosphorescence Lifetime Imaging

Measurement of PO_2 by PLI can be achieved by using a phosphorescent probe (Pd-porphine, excitation at 416 and 523 nm, emission at 687 nm) whose lifetime is dependent by the surrounding oxygen level.(Lo, et al. 1996) To spatially quantify the retinal vascular or tissue PO_2, the probe is either administered intravascularly (Shahidi, et al. 2006; Shonat and Kight 2003; Wilson, et al. 2005a) or intravitreally,(Shahidi, et al. 2010) respectively. A light source, such as a wide field illumination, is then aim at the retina to excite the probe to phosphoresce.(Shonat and Kight 2003; Wilson, et al. 2005a)

The phosphorescence of the probe will then be quenched by oxygen. As a result, an environment with a higher PO_2 will lead to a shorter phosphorescence lifetime, while an environment with a lower PO_2 will lead to a longer phosphorescence lifetime. This inverse relationship between the phosphorescence lifetime and PO_2 is governed by the Stern Volmer equation,(Lakowicz, et al. 1992; Shonat and Kight 2003)

$$PO_2 = (1/\kappa_Q)\cdot(1/\tau - 1/\tau_0) \qquad \text{(eq 8)}$$

where κ_Q (mm $Hg^{-1}\cdot\mu s^{-1}$) is the quenching constant for the triplet-state of Pd-porphine, τ (μs) is the phosphorescence lifetime, and τ_0 (μs) is the lifetime in a zero-oxygen environment. As a result, by determining the lifetime at varying locations in the retina using a camera, the PO_2 of the retinal vessels or tissue can be spatially quantified.

The phosphorescence lifetime of the probe can be quantified using either the time-domain or frequency-domain approach. The time-domain approach quantifies the intensity of the phosphorescence emission over time after a pulse of excitation light. The decay of the phosphorescence intensity over time can then be used to determine the phosphorescence lifetime by the following equation,(Sakadzic, et al. 2010; Shonat and Kight 2003)

$$I(t) = I_0\, e^{(-t/\tau)} \qquad \text{(eq 9)}$$

,where I(t) is the phosphorescence intensity at time t, I_0 is the initial intensity, and τ is the lifetime of the phosphorescent decay.

The frequency-domain approach also quantifies the intensity of the phosphorescence emission over time. However, the excitation light is continuous and sinusoidally modulated thereby producing a sinusoidal phosphorescence emission that has a lifetime-dependent phase delay relative to the sinusoidal excitation light, as shown in Figure 3A. The lifetime can therefore be derived from the phase delay by $\tan(\theta) = \omega*\tau$, where θ is the phase delay, ω is the frequency of the excitation light and τ is the lifetime. To determine the phase-delay (θ), phosphorescence intensities at multiple

phase-shifts are quantified and used to solved the coefficients of the following equations as proposed by Lakowicz et al,(Lakowicz, et al. 1992)

$$I(\theta_D) = a_0 + a_1 \times \cos(\theta_D) + b_1 \times \sin(\theta_D) \qquad \text{(eq 10)}$$

$$\text{,where} \qquad \theta = \tan (b_1/a_1)^{-1} \qquad \text{(eq 11)}$$

, where $I(\theta_D)$ is the intensity at phase delay θ_D, and a_0, a_1 and b_1 are coefficients that can be solved using linear least-squares by fitting $I(\theta_D)$ at 3 or more phase-shifts to equation 10. One advantage that the frequency-domain approach has over the time-domain approach is that the phase-delay at a given PO_2 is independent from the intensity of the excitation light. However, as this probe is not approved by the US Food and Drug Administration, PO_2 measurements based on PLI of the retina has only been performed in animals.(Mezu-Ndubuisi, et al. 2013; Shahidi, et al. 2009; Shonat and Kight 2003; Tsai, et al. 2003; Wilson, et al. 2005a)

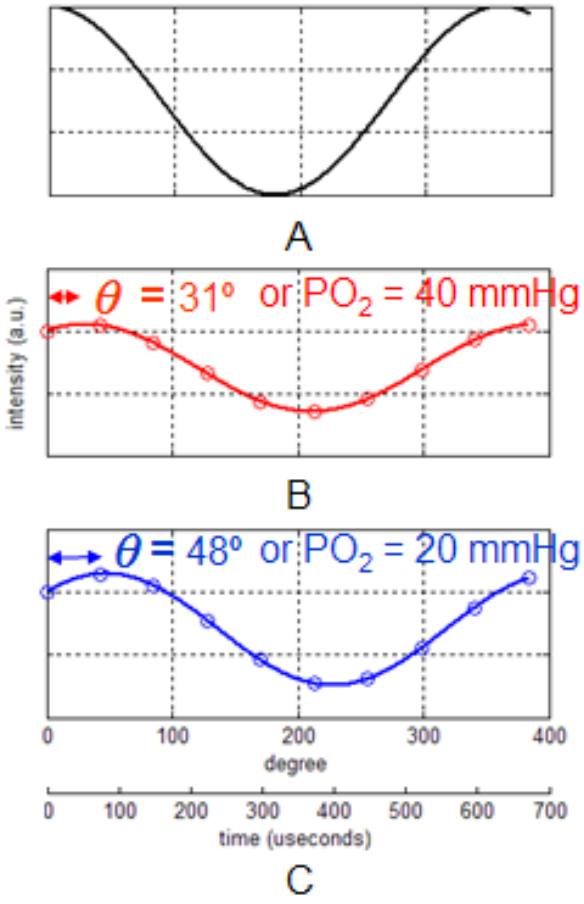

Fig. 3 A) Example light intensity over time of a sinusoidally modulated excitation laser (modulation frequency at 1.6 kHz). Example phosphorescence emissions over time in 2 mediums at PO2 values of 40 and 20 mmHg, and their respective phase delays (θ) due to the excitation laser are shown in B and C, respectively.

Given that the choroidal circulation is situated posterior to the retinal circulation, measurements of retinal vascular PO_2 by PLI using a conventional biomicroscope (with wild field illumination) will be influenced by the phosphorescence emitted from the choroidal vasculature. As a result, measurements of retinal PO_2, particularly in smaller retinal vessels, such as the microvessels between the major arteries and veins will not be accurate due to a weaker phosphorescence signal as compared to the underlying

choroidal phosphorescence.(Hardarson 2013; Linsenmeier 2012; Shonat and Kight 2003; Wilson, et al. 2005a)

In order to overcome the influence of choroidal phosphorescence from that of the retinal vessels, Shahidi et al have developed a system that can image depth-resolved phosphorescence in the chorioretinal vessels by combining PLI with optical sectioning.(Shahidi, et al. 2006; Shakoor, et al. 2006) In brief, an intensified charge-coupled device camera was attached to a slit lamp biomicroscope. Instead of using a wide field illumination as the excitation light source, a laser beam was used. This laser was first focused to a vertical line and then projected at an oblique angle on the retina, as illustrated in Fig 4A. Since the incident laser beam was at an angle with respect to the imaging path, phosphorescence emissions of the Pd-porphine from the retinal vessels will be depth-resolved. An example optical sectioned phosphorescence image of the retinal vasculature acquired by this system is shown in Fig 4B. Using this method, imaging of PO_2 in 3D can be achieved by moving the laser line laterally at incremental steps and acquiring optical sectioned phosphorescence images at each step.(Shahidi, et al. 2009)

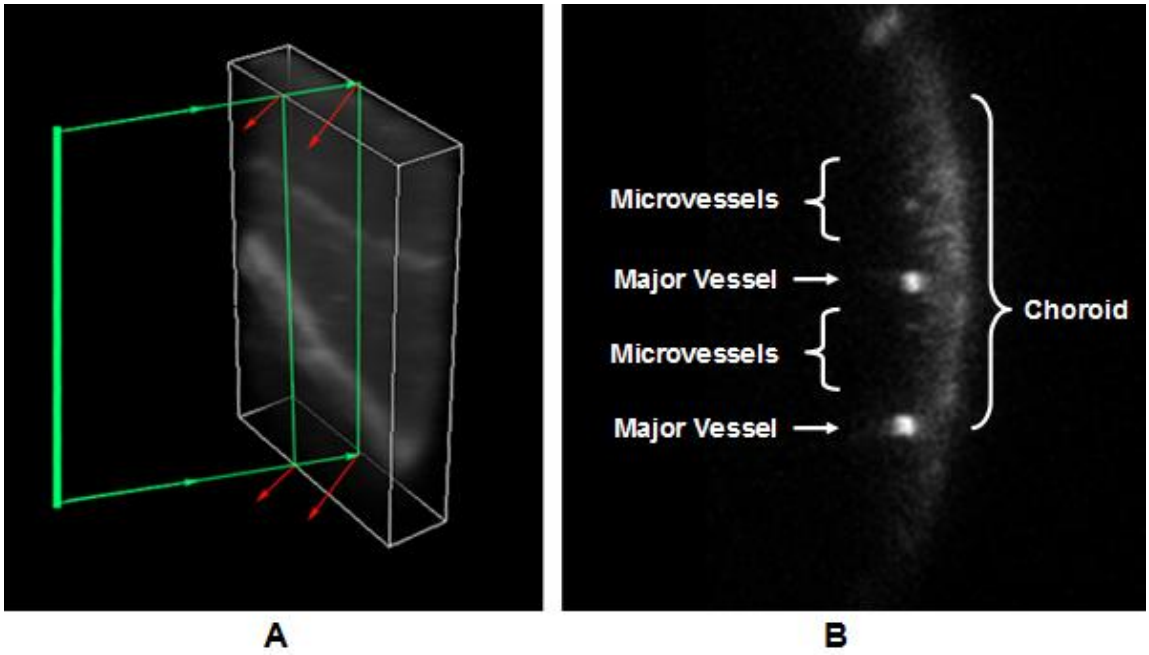

Fig. 4 A) An illustration of optical sectioning of the retina using a laser line as the excitation light. The laser is first focused to a line (thick green line) and then projected (thin green lines) to the retina (gray objects bounded by the white box) at an angle with respect to the imaging path (thin red lines). Due to this angle, the phosphorescence emission from the retinal vessels captured by the camera will be depth resolved. B) An example phosphorescence image of the retinal vessels acquired by optical sectioning PLI displaying phosphorescence from the retinal vessels (left of image) and the choroid (right of image).

III. A SEMI-AUTOMATED VESSEL LUMEN SEGMENTATION METHOD FOR QUANTIFICATION OF RETINAL VASCULAR PO_2 GENERATED BY 2D PLI

Introduction

Vascular abnormalities have been shown to be implicated in many retinal diseases.(Blair, et al. 2009; Connor, et al. 2009; Fraz, et al. 2012; Newman 2013; Riva, et al. 2005; Shakoor, et al. 2006) Specifically, vascular diameter, tortuosity, capillary density and oxygen level have been demonstrated to be altered in either diabetic retinopathy, retinopathy of prematurity or glaucoma.(Blair, et al. 2009; Connor, et al. 2009; Fraz, et al. 2012; Newman 2013; Riva, et al. 2005; Shakoor, et al. 2006) Quantification of these vascular attributes requires accurate delineation of the vascular boundaries through either manual or computer-assisted segmentation methods. While manual segmentation is generally considered as the gold standard for vessel segmentation,(Staal, et al. 2004) it suffers from intra- and inter-observer variability.(Bankhead, et al. 2012; Staal, et al. 2004) Furthermore, manual segmentation is a task that is both tedious and time consuming. As a result, a significant amount of research effort has been put towards the development of automated or semi-automated vessel segmentation methods.(Fraz, et al. 2012; Kirbas and Quek 2004; Suri, et al. 2002) However, to our knowledge, there have been no reported computer-assisted methods for segmenting retinal vascular lumens for quantification of vascular PO_2 generated by 2D PLI.

While it is possible to apply existing computer-assisted vessel segmentation methods to quantify the vascular PO_2 from images obtained by PLI, it may not be the most appropriate for the following reason. The majority of vessel segmentation methods rely only on the spatial information derived from one image. However, since quantifying

the vascular PO_2 by PLI requires acquisition of multiple phase-delayed phosphorescence images, an ideal vessel segmentation method should utilize spatial information extracted from all images.

In this chapter, a cross-correlation based semi-automated vessel lumen segmentation method for quantifying vascular PO_2 using multiple phosphorescence images was demonstrated. The semi-automated method was validated by quantifying the PO_2 from digital vascular phantoms. In addition, the method's performance was evaluated by comparing the variability of the quantified vascular PO_2 to those quantified manually in phosphorescence images acquired in the rat retina.

Materials and methods

Phantom and In-vivo Datasets

Eleven sets of vascular phantoms were generated for the validation of the semi-automated vessel lumen segmentation method. Each set of phantom contained 10 phase delayed phosphorescence images of a cross-sectional vascular lumen with a given PO_2 value. An example zero-phase delayed phosphorescence image of a phantom is shown in Fig 5A. The phosphorescence intensity in the vessel lumen at each phase delay was determined based on the phase delay and a PO_2 value, which varied for each phantom and ranged from 0 to 100 mmHg. White noise was added to the phantoms so that the signal to noise ratios matched those obtained in the actual rat retina (signal to noise ratio of 14.0 ± 0.5 dB, calculated from 3 sets of repeated images, each acquired from different rats).

Twelve sets of retinal vascular phosphorescence images obtained from 3 rats were used for the performance evaluation of the semi-automated method. Each set of images contained 10 phased-delayed phosphorescence images. An example zero-

phase delayed phosphorescence image is shown in Fig 5B. At least 3 major retinal vessels were imaged for each set of phosphorescence images. Overall, a total of 36 vascular PO_2 measurements were obtained from these images and used for the performance evaluation.

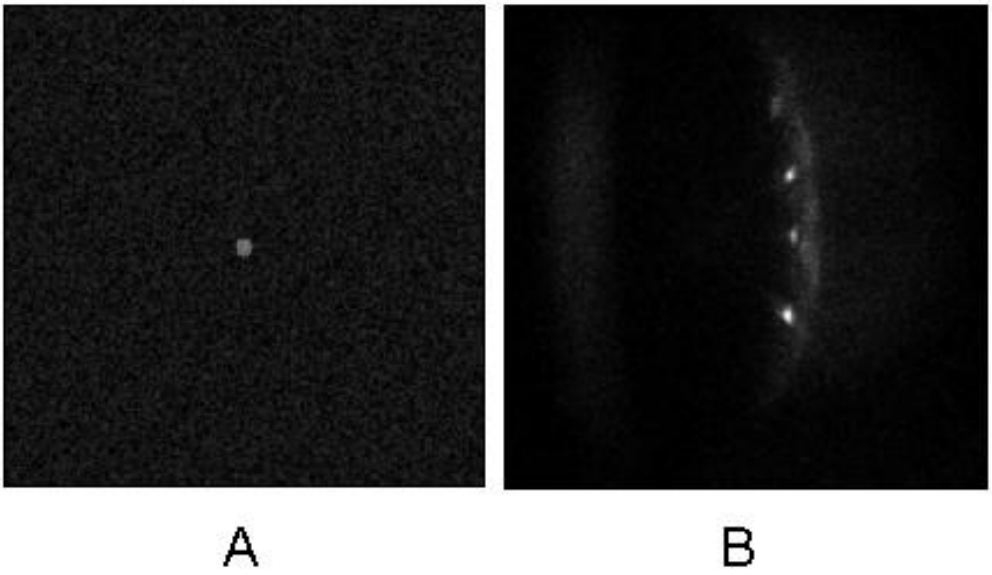

Fig. 5 Zero-phase delayed phosphorescence images of A) a vascular phantom and B) retinal vessels obtained in a rat.

Semi-automated Segmentation

The semi-automated vessel lumen segmentation method was based on cross correlation.(Alperin and Lee 2003) The rationale for using this method is as follows, and illustrated in Fig 6. Given a set of multiple phase-delayed phosphorescence images that bound a single cross sectional vascular lumen, as shown in Fig 6A, since the phosphorescent dye circulates inside the vessels and does not extravasate out to the retinal tissue,(Teng, et al. 2013) the phosphorescence intensity within the vessel would be relatively bright (such as locations near the red circle in Fig 6A) as compared to that

outside the vessel (such as locations near the blue square in Fig 6A). Furthermore, when the phosphorescence intensities within the vessel (red circle in Fig 6A) are plotted against the degree of phase-delays, the intensities would form a sinusoidal waveform (circles in Fig 6B). Conversely, when the phosphorescence intensities outside the vessel (blue square in Fig 6A) are plotted in the same fashion, it will not resemble a sinusoidal waveform due to the absence of the phosphorescent dye (squares in Fig 6B). Hence, the vessel within the images can be located by searching for pixels exhibiting similar sinusoidal waveforms by using cross correlation. Specifically, given a set of phase delayed phosphorescence images, P, and a reference sinusoidal waveform, R, a cross correlation map can be calculated using the following equation,

$$C_{xy} = \sum_{i=1}^{N} P_{xyi} \cdot R_i \qquad \text{(eq 1)}$$

where C_{xy} is the pixel intensity at row x and column y of the cross correlation map, P_{xyi} is the phosphorescence intensity at i^{th} phase-delay at row x and column y, and R_i is the mean intensity at i^{th} phase-delay of the reference waveform. The reference waveform was obtained based on the mean intensities at varying phase delays of pixels with a higher intensity at the zero-phase delayed phosphorescence image. The final cross correlation map is then normalized to range from 0 to 1. An example cross correlation map is shown in Fig 6C, locations with intensities closer to 1 indicate higher cross correlations with the reference waveform, and therefore are more likely to be within the vessel. A threshold for the cross correlation map was then determined using Otsu's binerization method,(Otsu 1975) and locations with cross correlations above the threshold were designated as locations within the vessel of interest (white pixels in Fig 6D). Finally the mean phosphorescence intensities at varying phase delays within the vessel of interest (crosses in Fig 6B) were obtained and used to determined the vascular PO_2,(Shonat and Kight 2003) as described in Chapter II.

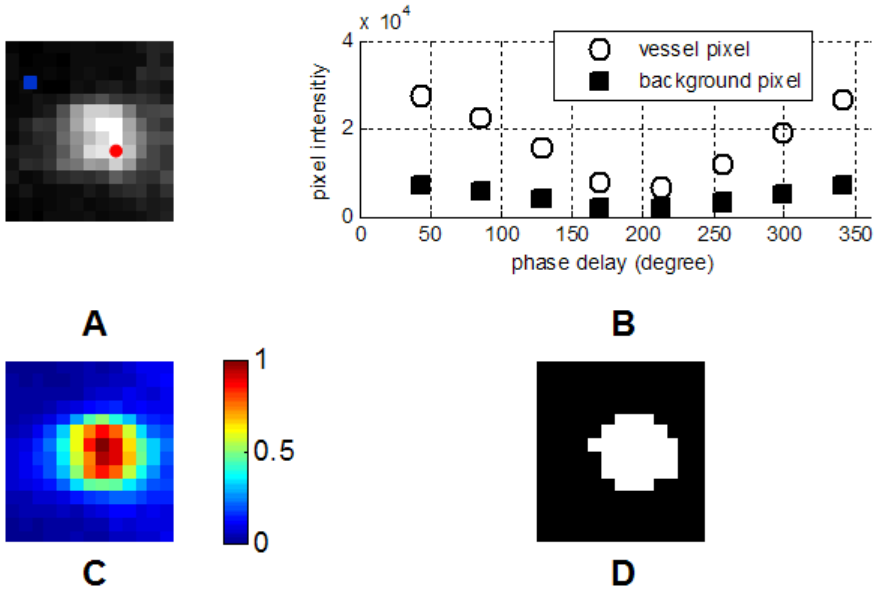

Fig. 6 A) A phosphorescence image of a cross sectional vascular lumen at zero-phase delay. The red circle and blue square indicate locations in the vessel and in the background, respectively. B) Phosphorescence intensities plotted against the degree of the phase delays of a location within the vessel (circles, corresponding to the red circle in A), in the background (squares, corresponding to the blue square in A). C) The cross correlation map obtained based on the multiple phase delayed phosphorescence images of the vessel shown in A. D) A binary image, with white pixels representing locations with a higher cross correlation as compared to pixels with lower cross correlation based on an automatically obtained threshold.

Validation and Performance Evaluation

To valid the semi-automated method, PO_2 of the vascular phantoms were quantified semi-automatically. The quantified PO_2 values were correlated with the actual PO_2. The differences between the quantified and actual PO_2 were also calculated. In addition, the performance of the semi-automated method was compared with that of the manual method using retinal vascular phosphorescence images acquired in rats. Specifically, the two methods were compared based on the inter- and intra-observer variabilities from vascular PO_2 quantified by two observers, and also the time to segment the vessels by these observers. Each observer quantified the vascular PO_2 twice (2

repeated measurements) for each method at one week apart. The intra-observer variabilities of the two methods were assessed using the Bland and Altman analysis,(Altman and Bland 1983) i.e. plotting the average against the difference of repeated measurements, and then calculating the 95% confidence interval (mean±1.96*SD of the difference of the repeated measurements). The naming conventions for the manual segmentation are M11 and M12 for the first and second repeated measurements for the 1st observer, respectively, and M21 and M22 for the second observer, respectively. The letter "M" is replaced with the letter "A" for the semi-automated method. Similarly, inter-observer variabilities of the 2 methods were also assessed with the Bland and Altman analysis using the average of repeated measurements between observer 1 and 2, i.e., M1 = (M11+M12)/2, and comparing M1 with M2. The segmentation time per vessel were also recorded and compared between the two methods using paired Student's t-test.

Results

Validation

The relationship between the semi-automatically quantified and actual PO_2 values of the vascular phantoms is shown in Fig 7. The quantified PO_2 values were highly correlated to the actual PO_2 values ($R^2 = 0.99$; $P < 0.001$). The difference between the quantified and actual PO_2 values were on average 0.6 ± 0.8 mmHg (N = 11).

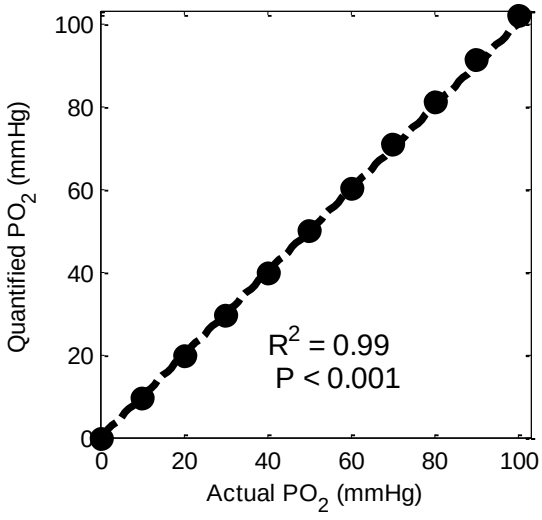

Fig. 7 The actual PO2 of the vascular phantoms plotted against the semi-automatically quantified PO2. The correlation coefficient and the corresponding P-value between the actual and quantified PO2 values are displayed. The line of identity is indicated by the dashed line.

Performance Evaluation

Example Bland and Altman plots of the repeated measurements obtained by one observer using the manual and the semi-automated methods are shown in Fig 8. As shown by the ranges of the confidence intervals (dashed lines) in the Bland and Altman plots, repeated measurements obtained using the semi-automated method was more consistent than those when the manual method was used for this observer. The results of the Bland and Altman analysis are shown in Table II. The means of differences between the repeated measurements were less or equal to 0.35 mmHg, indicating there were minimal bias between trials for both manual and semi-automated methods. For both observers, the ranges of the 95% confidence interval were smaller when the semi-automated method was used. Similarly, when comparing M1 versus M2 and A1 versus A2, the ranges of the 95% confidence interval were also smaller for the semi-automated method. The segmentation time was significantly less when the semi-automated

method was used as compared to when the manual method was used for every trial for both observers ($P<0.001$; N = 36 vessels). On average, the segmentation time was 4 ± 1 seconds per vessel when the semi-automated method was used, which was about 40% less than when the manual method was used (7 ± 1 seconds per vessel).

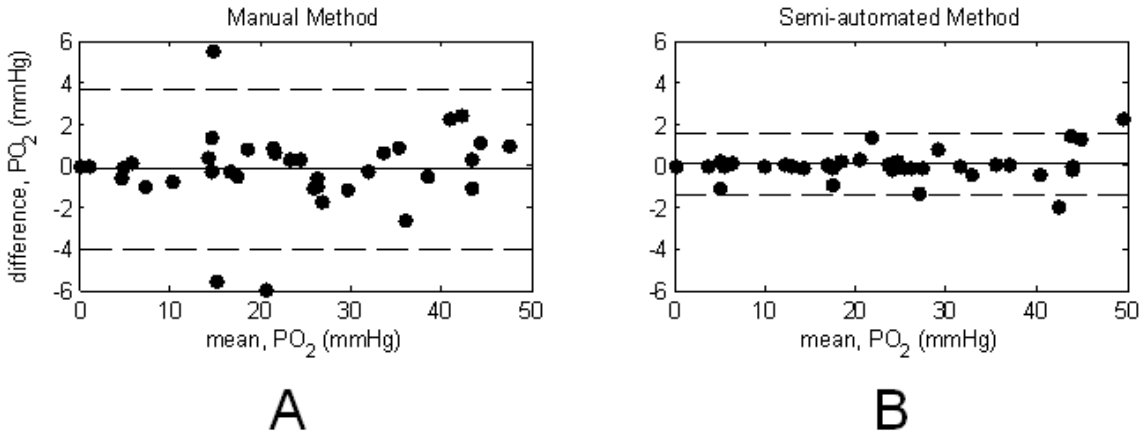

Fig. 8 Bland and Altman plots of the repeated measurements obtained by one observer using the manual (A) and the semi-automated (B) methods. The solid and dashed lines are the mean of difference from the repeated measurements and the corresponding 95% confidence interval, respectively.

TABLE II THE MEAN ± SD DIFFERENCE BETWEEN MEASUREMENTS AND THE CORRESPONDING 95% CONFIDENCE INTERVAL.

	Difference in PO_2 (mmHg, Mean ± SD)	95 % Confidence Interval in PO_2 (mmHg)
Intra-observer Evaluation		
M11, M12	-0.16 ± 1.94	-3.97 to 3.66
M21, M22	0.35 ± 2.29	-4.14 to 4.84
A11, A12	0.05 ± 0.76	-1.42 to 1.54
A21, A22	-0.10 ± 0.56	-1.21 to 1.00
Inter-observer Evaluation		
M1, M2	0.12 ± 1.82	-3.45 to 3.68
A1, A2	0.00 ± 0.37	-0.73 ± 0.72

Discussion

Segmentation of vascular boundaries from retinal images is a necessary step for quantification of morphological and functional attributes of retinal vessels. Since the quantified attributes are dependent on the segmentation results, use of semi-automated segmentation methods, as compared to manual segmentation, could potentially increase the repeatability of the parameters to be quantified. In this chapter, a semi-automated method for segmenting vascular lumens for quantification of vascular PO_2 from phosphorescence images was proposed. The semi-automated method was demonstrated to be superior to the manual method in terms of reduced variability and faster segmentation time.

The validation of the semi-automated method using the vascular phantoms demonstrated the quantified vascular PO_2 was highly correlated to the actual PO_2 values. Furthermore, the mean difference between the quantified and actual vascular PO_2 was less than 1 mmHg, indicating the semi-automated method was able to accurately quantify the vascular PO_2 from phosphorescence images.

Based on the performance evaluation, when the semi-automated method was used, the 95% confidence intervals were smaller as compared to those when the manual method was used, indicating the intra-observer variability was lower for the semi-automated method. Similarly, based on the inter-observer evaluation, the 95% confidence interval by the semi-automated method was also smaller than that by the manual method, indicating the inter-observer variability was lower for the semi-automated method. The reduced intra- and inter-observer variabilities for the semi-automated method suggest use of the proposed semi-automated method will increase the repeatability of the quantified vascular PO_2. In addition to the increased repeatability, the semi-automated method was also able to reduce the segmentation time by about 40%, which will aid in streamlining the vascular PO_2 quantification process.

In summary, this chapter demonstrated a novel semi-automated vascular lumen segmentation method for quantification of vascular PO_2. This semi-automated method was demonstrated to have higher repeatability and was faster as compared to when the manual method was used. The increase in repeatability will help in detecting smaller vascular PO_2 changes due to altered physiologic and pathologic conditions.

IV. A SEMI-AUTOMATED VESSEL TRACKING METHOD FOR QUANTIFICATION OF RETINAL VASCULAR PO_2 GENERATED BY 3D PLI

Introduction

The amount of oxygen extracted locally by any tissue is reflected by the vascular PO_2 changes along nearby vessel segments.(Boron and Boulpaep 2005; Tsai, et al. 2003) Hence, measurements of vascular PO_2 changes along retinal vessels could help gain fundamental knowledge of the local oxygen transport in the retina. However, due to difficulties in measuring the microvascular PO_2 in the living retina, few studies have investigated the changes of PO_2 along the retinal vessels.(Buerk, et al. 1993; Hardarson, et al. 2006; Shakoor, et al. 2006) More recently, Shahidi et al has developed an optical section PLI system that enabled imaging of the retinal vascular PO_2 in 3D.(Shahidi, et al. 2009)

While optical section PLI allows imaging of the retinal vascular PO_2, quantification of the vascular PO_2 along the vessels from these 3D images would require knowledge of the vessel geometry. Therefore, vessel tracking (obtaining the vessel segmentation and determining how the vessel is traversing) will need to be performed. Given that the vessels traverses in 3D, manually tracking these vessels will be a task that is both challenging and labor intensive. As a result, in order to efficiently quantify the PO_2 from the imaged retinal vessels by optical section PLI, use of an automated or semi-automated vessel tracking method is desired.

To our knowledge, there have been no previously published automated or semi-automated methods for quantifying vascular PO_2 from 3D images obtained by optical section PLI. In this chapter, a semi-automated vessel tracking method for quantification of vascular PO_2 from 3D phosphorescence images will be demonstrated. The proposed

method will be assessed by evaluating its accuracy of the quantified vascular PO_2 in a 3D vascular phantom.

Materials and Methods

Phantom and In-vivo Datasets

A 3D vascular PO_2 phantom (25x34x70 voxels) was generated for the validation of the semi-automated vessel tracking method. The phantom contained a single vessel with varying PO_2 along the vessel as shown in Fig 9. The diameter of the vessel was 9 pixels, a width comparable to those of major vessels in rats acquired using the optical section PLI system. The PO_2 varied along the vessel, and ranged from 85 mmHg at one end of the vessel to 25 mmHg to the other end of the vessel. In addition to the 3D phantom, an actual zero-phase delayed phosphorescence volume acquired from a rat retina was used for development of the interactive vessel segmentation software.

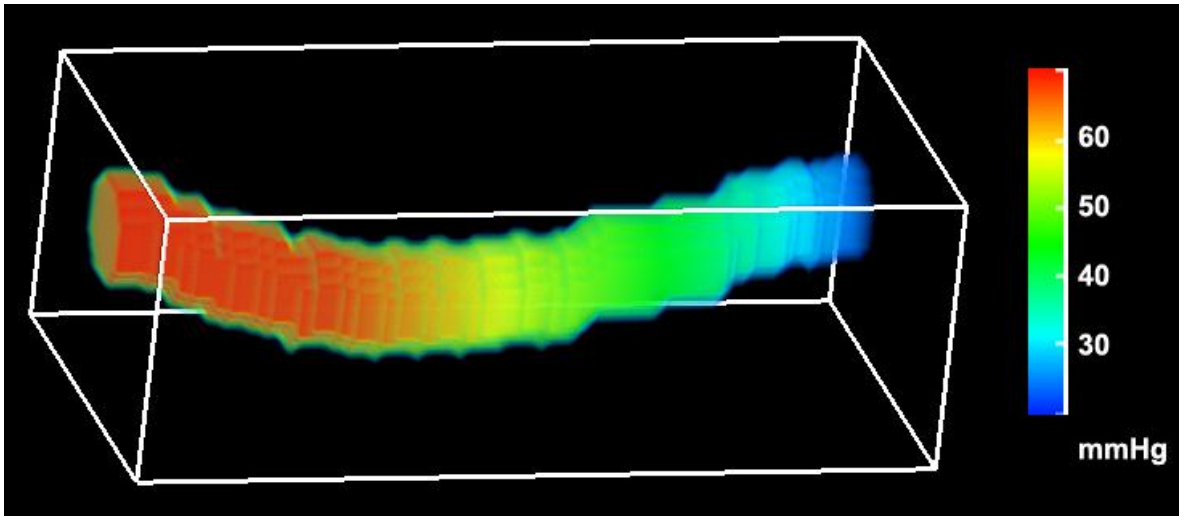

Fig. 9 The 3D vascular PO2 phantom, containing a single vessel segment with PO2 varying from 85 to 25 mmHg, as indicated by the pseudo-color and the corresponding colorbar.

Interactive Vessel Segmentation Software

An interactive vessel segmentation software was implemented in Matlab for delineating individual vessel segments from the zero-phase delayed phosphorescence volume. The software interface is shown in Fig 10. Using maximum intensity projection,(Sun and Parker 1999) the zero-phase delayed phosphorescence volume is displayed on the software interface from 3 different viewing angles. Based on the 3 views, the user can create a rough segmentation of the vessel by selecting a phosphorescence intensity threshold. Voxels with phosphorescence intensities above that threshold would then be selected as voxels within the vessel and masked in red (Fig 10, solid arrow). For each view, the masked volume is also displayed adjacent to the original volume (Fig 10, hollow arrow). The rough segmentation can then be refined to a specific vessel segment by including or excluding part of the mask based on a user-defined polygon illustrated by red lines and green dots (Fig 10, hollow arrow). The refining process can be iteratively performed until the segmentation best represents the contour of the vessel of interest.

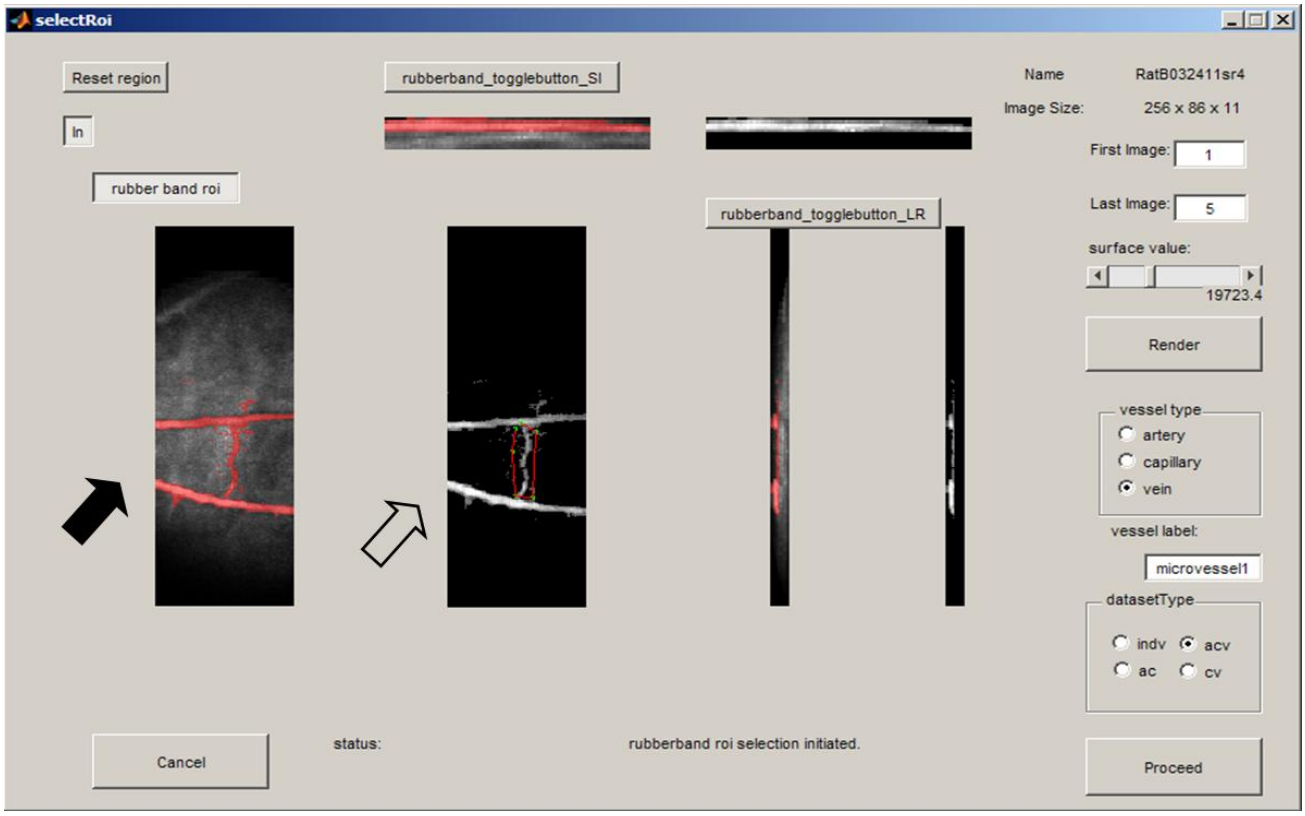

Fig. 10 The interface of the vessel segmentation software.

Vessel Centerline Extraction and Vascular PO_2 Quantification

The process for the extraction of vessel centerline is summarized in Fig 11 and has been previously described.(Teng, et al. 2011; Teng, et al. 2012) In brief, using manually determined vessel upstream and downstream points, and a binary volume obtained from the vessel segmentation, two distance fields were generated based on distance transformation.(Borgefors 1986; Borgefors 1996; Zhou and Toga 1999) The first field was a single-seeded field (SF), generated using the binary volume as the initial distance field and the downstream point as the initial seed. The second field was a boundary-seeded field (BF), generated also using the binary volume as the initial distance field and the vessel borders as the initial seeds. Example representative 2D images of a binary volume, and its corresponding SF and BF are shown in Fig 12. The

voxel intensities inside the SF represent how far each vessel voxel is relative to the downstream point, while those inside the BF approximate the shortest distance to the vessel boundary for each vessel voxel. Based on the two distance fields, a skeleton was extracted by iteratively traversing through descending values in the SF starting from the upstream point to the downstream point, which has the lowest value in the SF. In order to maintain the centeredness of the skeleton, each skeleton point was shifted locally so that it is a local maxima in the BF as shown by the skeleton overlaid on the BF in Fig 12.

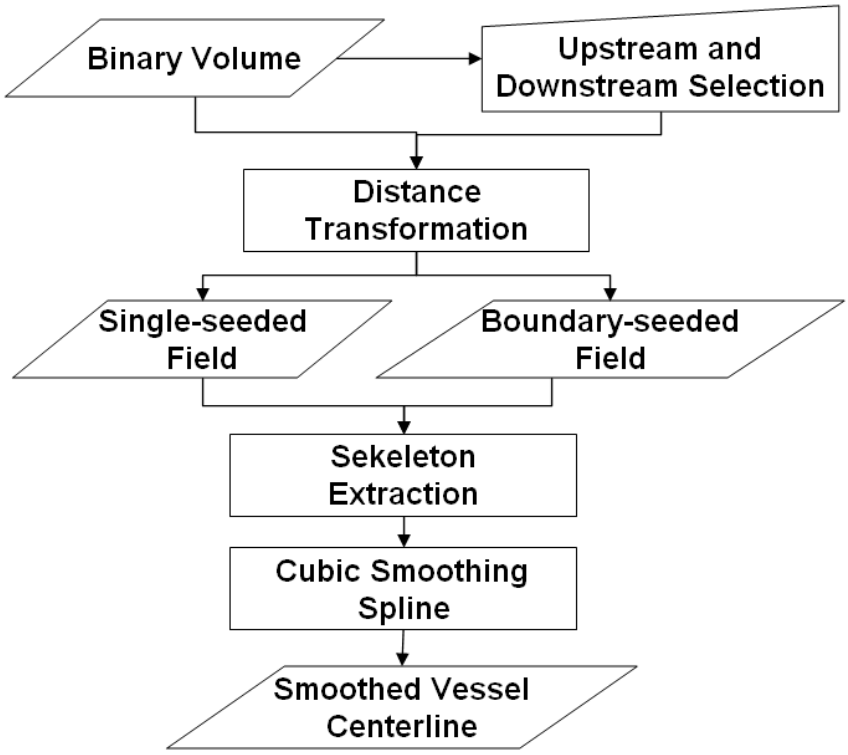

Fig. 11 A flow chart of the vessel centerline extraction process.

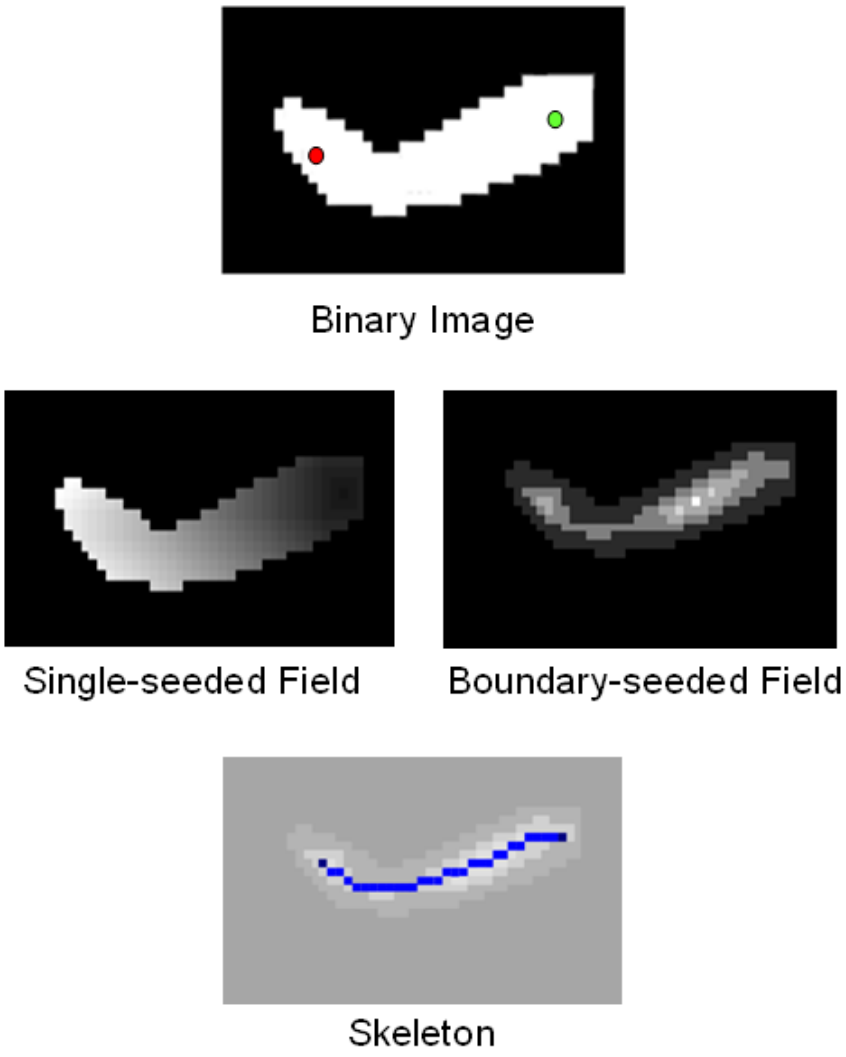

Fig. 12 Example images and data created during the vessel centerline extraction process. A) The initial binary image with the manually determined downstream and upstream points, indicated by the green and red circles, respectively. B) Two distance fields, single-seeded and boundary-seeded fields, were generated by distance transformation. C) The extracted skeleton (blue line), overlaid on a grayed-out boundary-seeded field. Note how the skeleton is situated at the local maximums of the boundary-seeded field.

The extracted skeleton was smoothed with cubic smoothing spline to generate the final vessel centerline. In brief, cubic smoothing spline solves for piecewise cubic polynomials by minimizing L, which is defined as follows,(De Boor 2001)

$$L = \lambda \sum_{i=0}^{n} (y_i - S_i)^2 - (1-\lambda) \int_{x_0}^{x_n} \{S''(x)\}^2 dx$$

Where y_i is the location of the skeleton point at index *i* in one dimension, n is the number of skeleton points, S_i or $S(x_i)$ is a cubic polynomial, and λ is a smoothing parameter. The value of λ was determined empirically so that the centerline will not have abrupt directional changes (physiologically impossible) and the distance between the resulting centerline and skeleton points are on average less than 1 voxel width apart. The smoothing process is performed to the skeleton points in all three dimensions.

The vascular PO_2 along the vessel was then quantified from the PO_2 volume by using the binary volume and the vessel centerline for identification of the vessel location and how the vessel is traversing, respectively. Each vessel centerline point was assigned a PO_2 based on the mean of PO_2 within the cross sectional vascular area perpendicular to the vessel axis. The quantification of the vascular PO_2 was then validated by correlating the quantified values with the actual PO_2 values in the vascular phantom. The absolute mean difference between the quantified and actual PO_2 was also calculated.

Results

Determination of λ

Example segments of the vessel centerlines at different λs are shown in Fig 13A. The mean difference between the vessel skeleton and centerlines at varying λs are plotted in Fig 13B. Abrupt changes in the vessel centerline were minimized when λ was greater than 0.1 (Fig 13A). At λs of 0.1 to 0.005, the mean difference between the skeleton and centerline varied minimally (0.6 to 0.7 voxel width), while at a λ of 0.001,

the mean difference approached 1, indicating the centerline was relatively not centered. Therefore the appropriate λ should be between 0.1 and 0.005. Hence, a λ of 0.01 was used for the cubic smoothing spline during the vessel centerline extraction process.

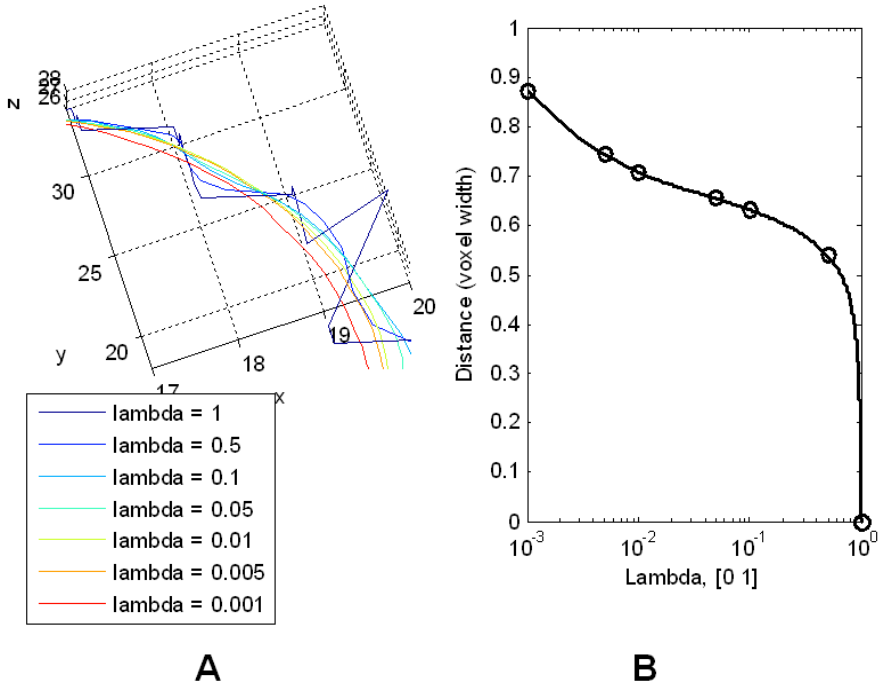

Fig. 13 A) Example segments of the vessel centerlines with different λs (lambda) displayed at an oblique viewing angle. B) Mean difference between the vessel skeleton and centerlines at varying λs plotted against the corresponding λ.

Validation of PO_2 Quantification

The extracted vessel centerline and the iso-surface of the binary volume of the 3D vascular PO_2 phantom are shown in Fig 14. The relationship between the quantified and actual vascular PO_2 values along the vessel centerline is shown in Fig 15. The quantified vascular PO_2 values were highly correlated with the actual PO_2 values (R^2 = 0.99; $P < 0.001$; $N = 85$). In addition, the absolute difference between the quantified and

actual PO_2 was 0.3 ± 0.2 mmHg (mean ± SD; N = 85), translating to a quantified error of 0.6% (100*[quantified PO_2 – actual PO_2]/[actual PO_2]).

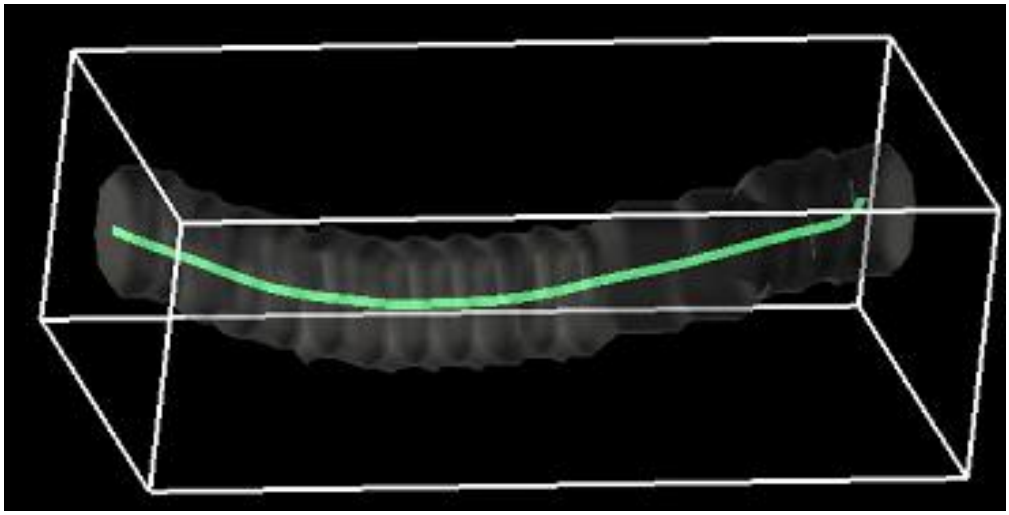

Fig. 14 The extracted vessel centerline (green line) and the iso-surface (gray shade) of the binary volume of the 3D vascular PO2 phantom.

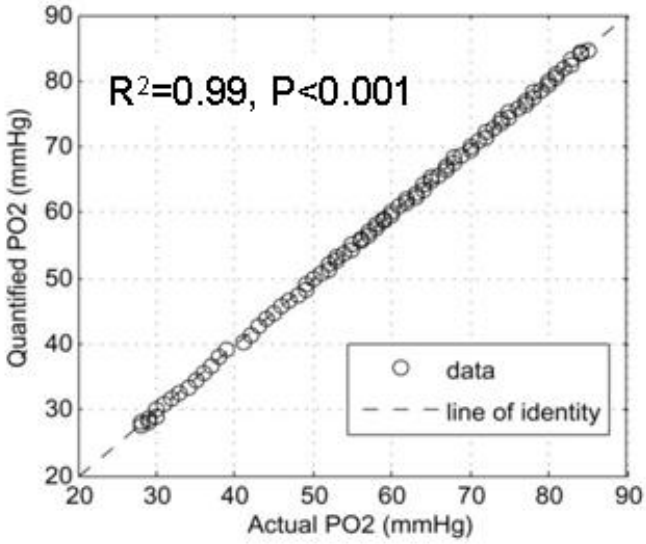

Fig. 15 The relationship between the actual and quantified PO2 values (circles). The correlation coefficient between the actual and quantified PO2, and the corresponding P-value are displayed. The dashed line indicates the line of identity.

Discussion

Investigation of changes in PO_2 along retinal vessels may help gain fundamental knowledge of oxygen transport in the retina. However, quantification of vascular PO_2 from images acquired by 3D PLI is hindered due to the labor intensive nature of manual vessel segmentation. In this chapter, a semi-automated vessel tracking method for 3D quantification of vascular PO_2 generated by optical section PLI was proposed and validated.

Evaluation of the semi-automated method demonstrated the quantified vascular PO_2 values from the 3D vascular phantom were highly correlated with the actual PO_2 and had an error rate of less than 1%. These findings indicate the semi-automated method is capable of accurately quantifying the vascular PO_2 acquired by 3D PLI. The semi-automatically obtained vessel segmentation and extracted vessel centerline can also be used to quantify other vascular parameters, such as the volume, diameter and tortuosity of the vessel segment. Furthermore, the extracted vessel centerlines could be used for image registration, which could aid in the investigation of vascular parameter changes in the same vessels over time.

The proposed vascular PO_2 quantification process could be further automated and improved. First, the vessel segmentation can be automated with methods including region growing or active contour.(Kirbas and Quek 2004) Second, the upstream and downstream points used for vessel centerline extraction can be automatically selected base on a priori knowledge of the shapes of the vessels. Finally, since the retinal vessels are in the form of a network, methods for detecting vessel branches and

organizing the hierarchy of theses vessels could potentially lead to a more in-depth understanding of the vascular PO_2 across the retinal microvasculature.

In summary, this chapter successfully validated a semi-automated vessel tracking method for quantification of vascular PO_2 from 3D phosphorescence images. As opposed to manual analysis, this method will enable a more streamlined data analysis process, thereby allowing users to efficiently investigate the oxygen transport in retinal microvasculature.

V. INNER RETINAL OXYGEN EXTRACTION FRACTION

Introduction

The maintenance of retinal tissue requires adequate delivery of oxygen by the retinal and choroidal circulations. Indeed, under a severe hypoxic or ischemic insult, retinal function is compromised (Linsenmeier 1990; Osborne, et al. 2004; Weidner 1976) and irreversible functional loss can occur shortly following retinal vascular non-perfusion.(Hayreh and Weingeist 1980; Hayreh, et al. 2004; Osborne, et al. 2004) Consequently, it would be advantageous to assess the status of the retina when impaired circulation is suspected.

Oxygen extraction fraction (OEF) is a parameter defined by the ratio of oxygen consumption (MO_2) to oxygen delivery (DO_2). Cerebral OEF measured by positron emission tomography and magnetic resonance imaging has been widely accepted as a valuable parameter for assessing tissue ischemia.(Baron and Jones 2012; Derdeyn 2007; Derdeyn, et al. 1999; Grubb, et al. 1998; Heiss and Herholz 1994; Muir, et al. 2006; Powers and Zazulia 2010; Yamauchi, et al. 1999) In fact, increased cerebral OEF, also termed “misery perfusion”, has been reported in subjects with acute ischemic stroke,(Heiss and Herholz 1994; Muir, et al. 2006; Powers and Zazulia 2010) and carotid occlusion.(Derdeyn 2007; Derdeyn, et al. 1999) Moreover, an increase in cerebral OEF has been shown to be an independent predictor of stroke.(Grubb, et al. 1998; Yamauchi, et al. 1999)

Due to similarities between cerebral and retinal tissues, measurement of OEF may also be useful for assessment of ischemia that occurs in many retinal diseases. However, currently available imaging modalities lack adequate resolution to quantify OEF in the retinal tissue. Alternatively, OEF can be expressed as the ratio of the

arteriovenous oxygen content difference to the arterial oxygen content based on Fick's principle,(Pittman 2011) as shown by the following equation.

$$OEF = \frac{MO_2}{DO_2} = \frac{Blood\ Flow \cdot Arteriovenous\ O_2\ Content\ \ Difference}{Blood\ Flow \cdot Arterial\ O_2\ Content} = \frac{Arteriovenous\ O_2\ Content\ \ Difference}{Arterial\ O_2\ Content} \quad (1)$$

Therefore, inner retinal OEF can be derived without direct measurements of MO_2 and DO_2.

In this chapter, a method for quantifying the inner retinal OEF based on retinal vascular oxygen tension (PO_2) imaging (Shahidi, et al. 2006) was demonstrated. The repeatability, spatial variation and hypoxia induced alterations of inner retinal OEF measurements were determined. This work has been previously published.(Teng, et al. 2013)

Materials and Methods

Animals

Ten Long Evans pigmented rats (weight, 444 ± 99 g, mean ± SD) were used in this study. The rats were treated in compliance with the ARVO Statement for the Use of Animals in Ophthalmic and Vision Research. Anesthesia was induced by intraperitoneal injections of ketamine (100 $mg \cdot kg^{-1}$) and xylazine (5 $mg \cdot kg^{-1}$), and maintained with supplemental injections of ketamine (20 $mg \cdot kg^{-1}$) and xylazine (1 $mg \cdot kg^{-1}$), as needed. The body temperatures of the rats were maintained at 37ºC using an animal holder with a copper tubing water heater. A catheter was placed in a femoral artery and connected to a pressure transducer. Blood pressure and heart rate of the rats were monitored with a data acquisition system (Biopac Systems, Goleta, CA) linked to a pressure transducer connected to the catheter.

The rats were mechanically ventilated with room air (21% O_2, normoxia) and then with 10% oxygen (hypoxia) through an endotracheal tube connected to a small animal

ventilator (Harvard Apparatus Inc., South Natick, MA). To verify the physiological condition, arterial blood was drawn from the femoral arterial catheter to measure systemic arterial oxygen tension (P_aO_2), carbon dioxide tension (P_aCO_2), and pH with a blood gas analyzer (Radiometer, Westlake, OH) and also hemoglobin concentration with a hematology system (Siemens, Tarrytown, NY). Animals were maintained normocapnic by adjusting the respiratory minute volume and performing blood gas analysis 5 minutes after each adjustment until P_aCO_2 was within the normal range of 35 to 45 mmHg.(Pilbeam and Cairo 2006) An oxygen sensitive molecular probe (Pd-porphine, Frontier Scientific, Logan, UT) was dissolved (12 $mg \cdot mL^{-1}$) in bovine serum albumin solution (60 $mg \cdot mL^{-1}$) and administered (20 $mg \cdot kg^{-1}$) through the femoral arterial catheter, typically 10 minutes prior to imaging. The probe binds to albumin and does not permeate from the normal vasculature to the retinal tissue. The pupils were dilated with 2.5% phenylephrine and 1% tropicamide. Glass cover slips and 1% hydroxypropyl methylcellulose were applied to the corneas to eliminate the refractive power and to prevent dehydration.

Retinal Vascular Oxygen Tension Imaging

Retinal vascular PO_2 was measured with a custom optical section PLI system developed by Shahidi et al.(Shahidi, et al. 2006) In short, a laser beam was focused to a vertical line, and projected at an oblique angle on the retina. An optical section phosphorescence image of the retinal vasculature was acquired with an intensified charge-coupled device camera attached to a slit lamp biomicroscope. Since the incident laser beam was at an angle with respect to the imaging path, phosphorescence emissions of the Pd-porphine from the retinal vessels were depth-resolved. Phosphorescence lifetime was determined using a frequency-domain approach and converted to PO_2 measurements using the Stern-Volmer relationship defined by PO_2 =

$(1/\kappa_Q)\cdot(1/\tau-1/\tau_0)$, where κ_Q ($mmHg^{-1}\cdot\mu s^{-1}$) is the quenching constant for the triplet-state of Pd-porphine, τ (μs) is the phosphorescence lifetime, and τ_0 (μs) is the lifetime in a zero-oxygen environment.(Lakowicz, et al. 1992; Shonat and Kight 2003) Measurements of PO_2 were obtained in a retinal sector, defined by a zone bounded by 2 major retinal arteries (PO_{2A}) with a major retinal vein (PO_{2V}) between the 2 arteries (Fig 16). Segmentation of each vessel lumen was performed using the semi-automated method proposed in Chapter III. Three repeated measurements were obtained at nasal and temporal retinal sectors, within 3 optic disc diameters (~ 600 μm) from the edge of the optic nerve head. A red-free retinal image was acquired for documenting the locations of the PO_2 measurements. Under both ventilation conditions, the laser power incident on the cornea was approximately 40 μW, which is safe for 1 hour of continuous viewing according to the American National Standard Institute for Safety Standards.(ANSI 2007)

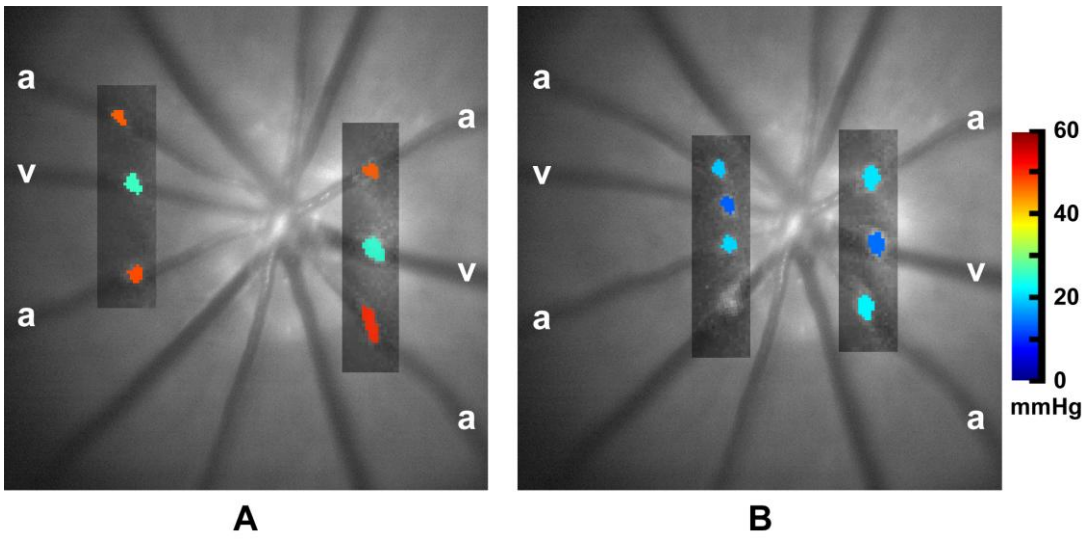

Fig. 16 Examples of cross-sectional vascular PO2 maps (shaded rectangles) superimposed on red-free retinal images in a rat under normoxia (A) and hypoxia (B). Maps depict PO2 in retinal arteries (a) and veins (v) in the nasal (right) and temporal (left) sides of the optic disc. Color bar displays PO2 in mmHg. Figure reprinted from Teng, et al.(Teng, et al. 2013)

Quantification of OEF

Based on retinal vascular PO_2 measurements, the O_2 content of blood was estimated as follows,

$$O_2\,content = O_{2\max} \times Hgb \times SO_2 + k \times PO_2 \quad (2)$$

where O_{2max} is the maximum oxygen carrying capacity of hemoglobin (1.39 $mLO_2 \cdot g^{-1}$),(Crystal 2001) Hgb is the measured hemoglobin concentration of arterial blood (13.9 ± 0.5 $g \cdot dL^{-1}$; N = 10), k is the oxygen solubility in blood (0.003 $mLO_2 \cdot dL^{-1} \cdot mmHg^{-1}$),(Crystal 2001) and SO_2 is the oxygen saturation. Based on vascular PO_2 and arterial blood pH measurements, SO_2 was calculated from the Hill equation which models the oxygen dissociation curve and is defined as $SO_2 = (PO_2/P_{50})^n/[1+ (PO_2/P_{50})^n]$, where n is an empirical constant taken to be 2.6 in rat,(Cartheuser 1993) and P_{50} is the PO_2 when SO_2 is 0.5 at a given pH.(Chen, et al. 2010)

Inner retinal OEF was quantified in a retinal sector as follows,

$$OEF = \frac{mO_{2A} - O_{2V}}{mO_{2A}} \quad (3)$$

where mO_{2A} is the mean arterial O_2 content of the 2 major arteries, and O_{2V} is the venous O_2 content. The mean arterial PO_2 of the 2 major arteries (mPO_{2A}) was also calculated.

Data Analysis

Repeatability of mPO_{2A}, PO_{2V} and OEF was determined by calculating the intraclass correlation coefficients (ICC) and the standard deviation (SD) of 3 repeated measurements obtained under normoxia at a retinal sector nasal to the optic disc. Repeated measurements of mPO_{2A}, PO_{2V} and OEF at each retinal sector were

averaged, and spatial variation was assessed by relating OEF measurements at nasal and temporal sectors using Pearson's correlation. In each rat, measurements of mPO_{2A}, PO_{2V} and OEF at nasal and temporal retinal sectors were averaged, and the mean values under normoxia and hypoxia were compared with paired Student's t-test. Statistical significance was accepted at $p < 0.05$.

Results

Repeatability and Spatial Variation

The ICCs and mean SDs (averaged over data in 10 rats) obtained from 3 repeated mPO_{2A}, PO_{2V} and OEF measurements in nasal retinal sectors under normoxia are shown in Table III. Measurements of mPO_{2A} and PO_{2V} were repeatable, with ICCs ≥ 0.86 and mean SDs ≤ 3 mmHg. Similarly, inner retinal OEF measurements were also repeatable (ICC = 0.83 and mean SD = 0.08). As anticipated, measurements of OEF at nasal and temporal retinal sectors were correlated under normoxia ($R = 0.71$; $p = 0.02$; $N = 10$).

TABLE III INTRACLASS CORRELATION COEFFICIENTS (ICC) AND MEAN STANDARD DEVIATIONS (SD), AVERAGED OVER DATA IN 10 RATS, BASED ON 3 REPEATED MPO2A, PO2V AND OEF MEASUREMENTS IN THE NASAL SECTORS UNDER NORMOXIA. TABLE REPRINTED FROM TENG, ET AL.(TENG, ET AL. 2013)

	ICC	SD
mPO_{2A}	0.86	3 mmHg
PO_{2V}	0.89	2 mmHg
OEF	0.83	0.08

Systemic Physiological Status

The systemic physiological status of the rats under normoxia and hypoxia is presented in Table IV. P_aO_2 under hypoxia (34 ± 4 mmHg) was significantly lower as compared to normoxia (93 ± 8 mmHg) ($p < 0.001$; N = 10). Due to controlled ventilation, P_aCO_2 under normoxia and hypoxia were similar ($p = 0.76$). Arterial blood pH, blood pressure and heart rate decreased significantly under hypoxia ($p \leq 0.001$).

TABLE IV THE SYSTEMIC PHYSIOLOGIC STATUS AND RETINAL VASCULAR PO_2 MEASUREMENTS UNDER NORMOXIA AND HYPOXIA. MEAN AND SD OF MEASUREMENTS IN 10 RATS ARE LISTED. ASTERISKS INDICATE STATISTICALLY SIGNIFICANT DIFFERENCES BETWEEN NORMOXIA AND HYPOXIA. TABLE REPRINTED FROM TENG, ET AL.(TENG, ET AL. 2013)

	Normoxia	Hypoxia	p-value
Systemic Physiologic Status			
P_aO_2 (mmHg)	93 ± 8	34 ± 4	< 0.001*
P_aCO_2 (mmHg)	40 ± 5	41 ± 5	0.76
pH	7.38 ± 0.05	7.31 ± 0.05	< 0.001*
Blood Pressure (mmHg)	113 ± 17	78 ± 22	0.001*
Heart Rate (beats·min^{-1})	214 ± 36	162 ± 45	0.002*
Retinal Vascular PO_2			
mPO_{2A} (mmHg)	44 ± 4	20 ± 4	< 0.001*
PO_{2V} (mmHg)	28 ± 5	11 ± 4	< 0.001*

Retinal Vascular PO_2 and OEF

Examples of cross sectional vascular PO_2 maps obtained in the same rat under normoxia and hypoxia are shown overlaid on the corresponding red-free retinal images in Fig 16. As expected, in both nasal and temporal sectors, mPO_{2A} was higher than PO_{2V} under both normoxia and hypoxia. Both mPO_{2A} and PO_{2V} decreased under hypoxia as compared to normoxia.

Measurements of mPO_{2A} and PO_{2V} averaged over all rats under normoxia and hypoxia are listed in Table IV. Under normoxia, $mPO2_A$ and $PO2_V$ were 44 ± 4 and 28 ± 5 mmHg, respectively (N = 10). Under hypoxia, both mPO_{2A} (20 ± 4 mmHg) and PO_{2V} (11 ± 4 mmHg) decreased significantly as compared to normoxia ($p < 0.001$). Mean measurements of inner retinal OEF under normoxia and hypoxia are shown in Fig 17. Mean inner retinal OEF was 0.46 ± 0.13 under normoxia and increased significantly to 0.67 ± 0.16 under hypoxia ($p < 0.001$; N = 10).

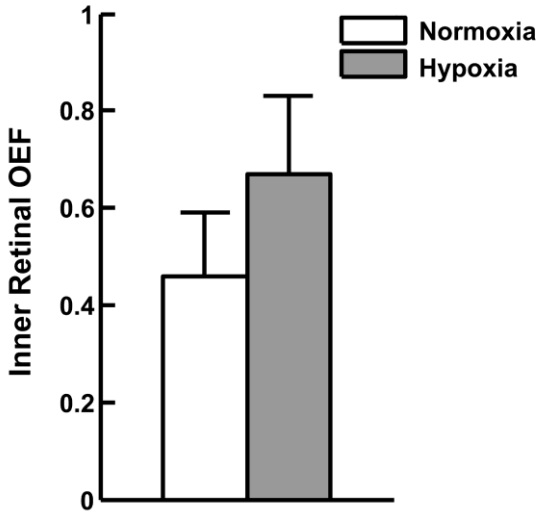

Fig. 17 Inner retinal oxygen extraction fraction (OEF) under hypoxia (0.67 ± 0.16) was significantly higher than under normoxia (0.46 ± 0.13) (mean ± SD; $p < 0.001$; N = 10). Figure reprinted from Teng, et al.(Teng, et al. 2013)

Discussion

Retinal ischemia is implicated in many retinal diseases that lead to visual impairment. However, methods that can quantitatively assess the retinal tissue status in vivo under ischemia are limited. One potential parameter is OEF, which indicates the adequacy of oxygen supply relative to the tissue's metabolic demand. In the current study, quantitative measurements of inner retinal OEF in rats based on retinal vascular PO_2 imaging was demonstrated. A significant increase in inner retinal OEF under systemic hypoxia was observed.

Inner retinal OEF measurements in the current study were compared to calculated retinal and measured cerebral OEFs due to a lack of published retinal data. Based on oximetry studies in healthy subjects,(Geirsdottir, et al. 2012; Hammer, et al. 2011; Hardarson, et al. 2006) the inner retinal OEF in human was computed to be 0.40, which is comparable to the current measurements of 0.46 in rats under normoxia. Additionally, inner retinal OEF measured under normoxia in the current study was in agreement with published cerebral OEFs (0.37 to 0.57).(Hoffman, et al. 1984; Ito, et al. 2004; Johannsson and Siesjo 1975; Kobayashi, et al. 2012; Magata, et al. 2003; McPherson, et al. 1986) The current finding of increased inner retinal OEF under systemic hypoxia was similar to elevated inner retinal OEF in chronic systemic hypoxia(Traustason, et al. 2011) and central retinal vein occlusion,(Hardarson and Stefansson 2010) calculated from oximetry data in humans. Moreover, this finding was also consistent with the response of cerebral OEF under hypoxia.(Hoffman, et al. 1984; Johannsson and Siesjo 1975; McPherson, et al. 1986)

An increase in inner retinal OEF can occur due to either an increase in retinal MO_2 or a decrease in DO_2. Under hypoxia, since MO_2 is unlikely to increase, the observed increase in inner retinal OEF would occur due to a decrease in DO_2 that can result from reductions in retinal blood flow and/or arterial blood oxygen content.(Wanek,

et al. 2013) Although retinal blood flow could in principle be affected by systemic blood pressure and/or blood pH, it was not likely influenced by these factors under the experimental conditions. Blood pressure remained within the autoregulatory range,(Davis, et al. 2008) even though it was reduced during hypoxia. Likewise, a change in blood pH was not expected to alter blood flow, according to findings in the brain.(Harper and Bell 1963; Hermansen, et al. 1984) On the other hand, hypoxia has been reported to increase retinal blood flow (Ahmed, et al. 2001; Nagaoka, et al. 2002; Pournaras, et al. 2008; Strenn, et al. 1997) which would tend to maintain DO_2. Nevertheless, the compensatory increase in blood flow may not be adequate to maintain DO_2, if the hypoxia is severe enough. In that case, because of reductions in retinal arterial blood oxygen content, DO_2 decreases thereby causing an increase in inner retinal OEF.

One factor that likely affected the results was that oxygen contents in retinal veins were estimated from the oxygen dissociation curve using the arterial blood pH. Since blood pH is expected to be lower in veins than in arteries,(Gibbs, et al. 1942; Oshima, et al. 2002) the actual venous oxygen contents were likely lower due to a right shift of the oxygen dissociation curve. As a result, the actual inner retinal OEF should have been higher than the reported values under normoxia. The right shift of the oxygen dissociation curve would be expected to be even more prominent during hypoxia due to increased anaerobic metabolism. Since OEF was underestimated under both ventilation conditions, this limitation likely did not affect the current finding of increased inner retinal OEF under hypoxia.

Measurements of inner retinal OEF may provide information about the retinal tissue status during ischemic insult complimentary to retinal blood flow measurements or conventional diagnostic tests, such as fundus photography and fluorescein angiography. An acute increase in retinal OEF indicates a state of misery perfusion, in which DO_2

declines, and thereby support for MO_2 becomes precarious. If DO_2 remains reduced chronically, irreversible anoxic damage may develop, leading to decreases in retinal MO_2 and OEF. Therefore, while OEF is elevated, retinal tissue may still remain viable,(McLeod 2012) thus potentially providing a window of opportunity for successful intervention, as has been demonstrated in cerebral tissue.(Durukan and Tatlisumak 2007; Fisher 1997; Heiss, et al. 1998) In the current study, inner retinal OEF was assessed under 2 ventilation conditions to establish a normal baseline and demonstrate a response to a severe hypoxic challenge. Additional studies that assess inner retinal OEF in response to varying levels of inspired oxygen may help establish a threshold at which OEF begins to increase due to maximized blood flow compensation. Furthermore, future studies are needed to provide knowledge of OEF response in experimental animal models of retinal vascular deficiency that may eventually be translated for clinical management of patients.

In summary, a method for quantitative measurement of inner retinal OEF in rats was demonstrated. In addition, OEF was observed to increase under acute systemic hypoxia. The method can be extended to provide a global assessment of inner retinal OEF by measuring O_2 contents in all major retinal blood vessels. Quantification of inner retinal OEF has potential value for providing information about the retinal energy metabolism under challenged physiological and pathological conditions.

VI. RESPONSE OF INNER RETINAL OXYGEN EXTRACTION FRACTION TO LIGHT FLICKER

Introduction

Stimulation of the retinal tissue with light flicker increases the inner retinal energy metabolism.(Bill and Sperber 1990; Wang and Bill 1997) This increase in energy metabolism is compensated by an augmented supply of oxygen and glucose due to increased blood flow in a process known as functional hyperemia.(Newman 2013; Riva, et al. 2005) Impaired functional hyperemia, as demonstrated by attenuated vasodilation during light flicker, has been reported in diabetic retinopathy(Bek, et al. 2008; Garhofer, et al. 2004b; Hammer, et al. 2012; Lasta, et al. 2013) and glaucoma,(Garhofer, et al. 2004a; Riva, et al. 2004) suggesting an incomplete compensatory blood flow response to increased energy metabolism. However, since no clinical methods are available for measurements of inner retinal energy metabolism, it is unknown if changes in oxygen metabolism and delivery (product of blood flow and arterial oxygen content) are matched in health and disease.

The relative changes of inner retinal oxygen metabolism (MO_2) and oxygen delivery (DO_2) during light flicker can be quantified by measurement of inner retinal oxygen extraction fraction (OEF), which is defined by the ratio of MO_2 to DO_2.(Pittman 2011) Without direct measurements of either MO_2 or DO_2, inner retinal OEF can be derived from measurements of arterial and venous oxygen levels based on Fick's principle.(Pittman 2011; Teng, et al. 2013) During light flicker, if OEF remains unchanged, then changes in MO_2 and DO_2 are matched, while an increase or decrease in OEF with light flicker would indicate either under or over compensation of MO_2 by DO_2, respectively.

In this chapter, the hypothesis that inner retinal OEF remains unchanged with light flicker, under both systemic normoxia and hypoxia was tested. The rationales for formulating this hypothesis are as follows. Under normal physiology (normoxia), the increase in MO_2 with light flicker should be matched by an increase in DO_2 due to vasodilation, thus resulting in no change in inner retinal OEF. Under a severe hypoxic challenge, even without light flicker, both MO_2 and DO_2 are significantly reduced.(Wanek, et al. 2013) With light flicker, no increase in DO_2 is expected due to hypoxia-induced maximized vasodilation and since the tissue under hypoxia is already deficient of oxygen, MO_2 is unlikely to increase. Consequently, inner retinal OEF is not expected to change with light flicker under hypoxia. To test this hypothesis, the response of OEF to light flicker was measured in rats under systemic normoxia and hypoxia by vascular oxygen tension (PO_2) imaging.

Materials and Methods

Animals

Ten Long Evans pigmented rats (weight 444 ± 99 g, mean ± SD; N = 10) were used in this study. Rats were cared for in compliance with the ARVO Statement for the Use of Animals in Ophthalmic and Vision Research. Anesthesia was induced with intraperitoneal injections of ketamine (100 $mg \cdot kg^{-1}$) and xylazine (5 $mg \cdot kg^{-1}$), and maintained with supplemental doses of ketamine (20 $mg \cdot kg^{-1}$) and xylazine (1 $mg \cdot kg^{-1}$). The body temperatures of rats were maintained at 37ºC using a heated animal holder. Blood pressure and heart rate were monitored continuously with a data acquisition system (Biopac Systems, Goleta, CA) linked to a pressure transducer connected to a catheter placed in a femoral artery.

Rats were ventilated first with room air (21% oxygen, normoxia) and then with 10% oxygen (hypoxia) through an endotracheal tube connected to a small animal ventilator (Harvard Apparatus Inc., South Natick, MA). Blood was drawn from the femoral arterial catheter to measure systemic arterial oxygen tension (P_aO_2), carbon dioxide tension (P_aCO_2), and pH with a blood gas analyzer (Radiometer, Westlake, OH) and determine hemoglobin (Hgb) concentration with the use of a hematology system (Siemens, Tarrytown, NY). Rats were maintained normocapnic by adjusting the respiratory minute volume and performing blood gas analysis 5 minutes after each adjustment until P_aCO_2 was within the range of 35 to 45 mmHg.

An oxygen sensitive molecular probe, Pd-porphine (Frontier Scientific, Logan, UT), was dissolved (12 $mg \cdot mL^{-1}$) in bovine serum albumin solution (60 $mg \cdot mL^{-1}$) and administered (20 $mg \cdot kg^{-1}$) through the femoral arterial catheter typically 10 minutes prior to imaging. The pupil was dilated with 2.5% phenylephrine and 1% tropicamide. During imaging, a glass cover slip and 1% hydroxypropyl methylcellulose were applied to the cornea to minimize the refractive power and prevent dehydration.

Retinal Stimulation by Light Flicker

Under each systemic oxygenation condition (normoxia and hypoxia), imaging was performed first under continuous light illumination (before flicker) and then under flickering light (during flicker). For light flicker stimulation, a filter with a transmission wavelength of 568 ± 5 nm was placed in front of the illumination housing of a slitlamp biomicroscope. A shutter attached to a solenoid was placed in the light path to flicker light at a frequency of 10 Hz. The light wavelength and flickering frequency were selected based on previous studies that showed a maximal or near maximal vascular response under these conditions.(Shakoor, et al. 2006; Shih, et al. 2011) The time-averaged light powers before and during flicker were matched by doubling the light

intensity during flicker. Imaging was performed before and 2 minutes after the initiation of light flicker.

Retinal Vascular Oxygen Tension Imaging

Retinal vascular PO_2 was measured with an optical section PLI system developed by Shahidi et al.(Shahidi, et al. 2006) In brief, using a laser line as the excitation light source, phosphorescence emission lifetimes were measured by a frequency-domain approach, and converted to PO_2 values using the Stern-Volmer relationship.(Shonat and Kight 2003) Since the incident laser was projected at an angle with respect to the imaging path, depth-resolved PO_2 measurements were obtained in major retinal arteries and veins. The laser power at the cornea was approximately 40 μW, which is safe for 1 hour of continuous viewing according to the American National Standard Institute for Safety Standards.(ANSI 2007) A red-free retinal image was acquired for documenting the locations of PO_2 measurements. Vascular PO_2 images were obtained at a nasal and a temporal sector relative to the optic disc. Each sector was bounded by 2 major arteries with a major vein between them. In each sector, 3 repeated images were acquired.

Oxygen Extraction Fraction

Based on Fick's principle,(Pittman 2011) inner retinal OEF was quantified in a retinal sector as proposed in Chapter V, using the following equation,

$$OEF = \frac{MO_2}{DO_2} = \frac{Blood\ Flow \cdot (O_{2A} - O_{2V})}{Blood\ Flow \cdot O_{2A}} = \frac{O_{2A} - O_{2V}}{O_{2A}}$$

where O_{2A} is the mean arterial O_2 content of 2 major arteries and O_{2V} is the venous O_2 content. The O_2 contents were calculated as O_{2max}* Hgb * SO_2 + k * PO_2, where O_{2max} is the maximum oxygen carrying capacity of Hgb (1.39 $mLO_2 \cdot g^{-1}$),(Crystal 2001) k is the

oxygen solubility in blood (0.003 $mLO_2 \cdot dL^{-1} \cdot mmHg^{-1}$),(Crystal 2001) and SO_2 is the vascular oxygen saturation. The vascular SO_2 was estimated based on the measured vascular PO_2 and blood pH, using an oxygen dissociation curve in rat.(Cartheuser 1993; Chen, et al. 2010) Arterial and venous SO_2 were estimated from the mean PO_2 in 2 major arteries (PO_{2A}) and the venous PO_2 (PO_{2V}) between the 2 arteries, respectively. Because O_{2V} cannot exceed O_{2A}, inner retinal OEF ranges from 0 to 1, following the equation above.

Statistical Analysis

Three repeated measurements of retinal oxygenation parameters (PO_{2A}, PO_{2V}, and OEF) were averaged for each sector. Values in nasal and temporal sectors were then averaged in each rat. A two-way repeated measures analysis of variance (ANOVA) was used to determine the effects of light flicker (before and during) and systemic oxygenation condition (normoxia and hypoxia) on each retinal oxygenation parameter. Statistical significance was accepted at $P < 0.05$.

Results

Systemic Physiological Status

The systemic physiological status of rats under normoxia and hypoxia are shown in Table IV. As expected, the systemic P_aO_2 under hypoxia was significantly lower as compared to that under normoxia ($P < 0.01$; $N = 10$). Since the ventilation was controlled, systemic P_aCO_2 was not different under the two systemic oxygenation conditions ($P = 0.76$). However, under hypoxia, arterial blood pH, blood pressure and heart rate decreased significantly ($P < 0.01$).

Retinal Oxygenation Parameters

Retinal oxygenation parameters before and during light flicker, and their differences (during minus before) under normoxia and hypoxia are listed in Table V. There was a significant effect of light flicker on PO_{2V} ($P < 0.01$; $N = 10$), but not on PO_{2A} ($P = 0.71$). During light flicker, PO_{2V} decreased on average by 1.3 mmHg and 1.2 mmHg under normoxia and hypoxia, respectively. As expected, there were significant effects of systemic oxygenation on both retinal PO_{2A} and PO_{2V} ($P < 0.01$), as reported in chapter V.

TABLE V RETINAL OXYGENATION PARAMETERS (MEAN ± SD; N = 10) BEFORE AND DURING LIGHT FLICKER AND THEIR DIFFERENCE (DURING MINUS BEFORE) UNDER TWO SYSTEMIC OXYGENATION CONDITIONS (SOC), NORMOXIA (N) AND HYPOXIA (H).

	SOC	Before Flicker	During Flicker	Difference	ANOVA P-Value		
					Flicker	SOC	Flicker x SOC
PO_{2A} (mmHg)	N	44 ± 4	44 ± 4	0.1 ± 1.9	0.71	<0.01	0.92
	H	19 ± 4	20 ± 3	0.1 ± 0.7			
PO_{2V} (mmHg)	N	28 ± 5	27 ± 4	-1.3 ± 1.0	<0.01	<0.01	0.80
	H	11 ± 4	10 ± 5	-1.2 ± 1.8			
OEF	N	0.46 ±0.13	0.50 ±0.11	0.05 ± 0.04	0.02	<0.01	0.52
	H	0.67 ±0.16	0.74 ±0.14	0.07 ± 0.11			

Measurements of inner retinal OEF in individual rats before and during light flicker under normoxia and hypoxia are plotted in Figure 18. During light flicker, OEF

increased in 8 of 10 rats and in 9 of 10 rats under normoxia and hypoxia, respectively. There were significant main effects of both light flicker and systemic oxygenation on OEF ($P \leq 0.02$; $N = 10$). However, the interaction effect was not significant ($P = 0.52$), indicating similar responses of OEF to light flicker under both systemic oxygenation conditions. Before light flicker, mean inner retinal OEF measurements were 0.46 and 0.67 under normoxia and hypoxia, respectively. During light flicker, inner retinal OEF increased to 0.50 (11%) and 0.74 (10%) under normoxia and hypoxia, respectively.

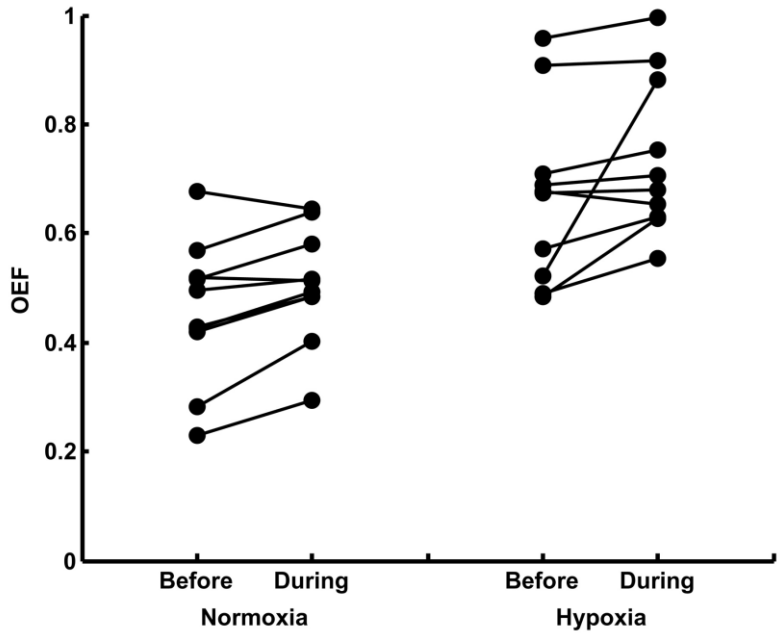

Fig. 18 Measurements of inner retinal OEF in individual rats before and during light flicker under systemic normoxia and hypoxia. During flicker, OEF increased in 8 of 10 rats and in 9 of 10 rats under normoxia and hypoxia, respectively. Inner retinal OEF before light flicker have been previously published.(Teng, et al. 2013)

Discussion

Measurement of inner retinal OEF provides information about the matching of oxygen metabolism and delivery. The reported finding of increased inner retinal OEF

during light flicker under both normoxia and hypoxia indicates MO_2 was under compensated by DO_2.

Under normoxia, the response of inner retinal OEF to light flicker indicates the increase in MO_2 was not matched by an increase in DO_2. In agreement with findings of the present study, under compensation of MO_2 by DO_2 during light flicker has been shown by a decrease in inner retinal or optic nerve head PO_2 in rats and cats,(Ahmed, et al. 1994; Buerk, et al. 1998; Buerk and Riva 2002; Lau and Linsenmeier 2012) and an increase in arteriovenous PO_2 difference in spontaneously breathing rats.(Shakoor, et al. 2006) Conversely, in humans, light flicker caused an increase in retinal venous SO_2, while arterial SO_2 did not change,(Hammer, et al. 2011) thereby suggesting over compensation of MO_2 by DO_2. The different findings of these studies are likely attributable to variations between species and experimental protocols. Nevertheless, these studies investigated functional hyperemia in healthy retinas. Therefore, in both rats and humans, compensation by DO_2 should be sufficient to maintain the normal increase in MO_2 and energy dependent neural activity induced by light flicker. The current finding of increased OEF coupled with the known increase in blood flow (and DO_2) confirms MO_2 increases with light flicker.

Under hypoxia, inner retinal OEF increased with light flicker, contrary to the proposed hypothesis that OEF would remain unchanged which was based on the following line of reasoning. Under this severe hypoxic challenge, inner retinal MO_2 was previously found to be reduced to approximately one third of that under normoxia,(Wanek, et al. 2013) thus the tissue was already deficient in oxygen and MO_2 would not be able to increase with light flicker. Furthermore, vasodilation was likely maximized due to hypoxia, thus precluding an increase in DO_2. As a result, with no change in MO_2 and DO_2, OEF was expected to remain unchanged. Nonetheless, inner retinal OEF was found to increase with light flicker, which is most likely attributed to an

increase in MO_2, since DO_2 is unlikely to decrease with light flicker. The question then arises as to how oxygen extraction and MO_2 could increase with light flicker, given the existing oxygen deficiency in the retina under hypoxia. One explanation could be that even under systemic hypoxia, tissue near blood vessels may still be adequately supplied with oxygen and thus could respond to light flicker with increased MO_2, whereas tissue farther away from blood vessels is unable to respond to light flicker because of hypoxia. According to Fick's laws of diffusion, with an increase in MO_2, the oxygen gradient from the vessel wall into the tissue would steepen, thereby increasing both the rate of oxygen loss from blood and OEF.(Tsai, et al. 2003) Simultaneously, the lower oxygen content of blood under hypoxia coupled with the steeper oxygen gradient with light flicker will cause less tissue to be oxygenated, and thus exacerbate overall tissue hypoxia.

Although the response of inner retinal OEF to light flicker were similar under normoxia and hypoxia, the corresponding increases in MO_2 may have been different. Under hypoxia, compensation by DO_2 was likely lower due to maximized vasodilation, hence a given increase in OEF would result from a smaller change in MO_2. The light flicker-induced increase in MO_2 can be estimated based on Fick's principle (MO_2 = OEF*O_{2A}*blood flow).(Pittman 2011) Under normoxia, the measured increase in OEF (0.46 to 0.50) and unchanged O_{2A} (unchanged PO_{2A}), along with a previously reported increase in blood flow (9.9 to 13.5 µL/min),(Shih, et al. 2013) yielded an estimated light flicker-induced MO_2 increase of 48%. This value is in agreement with an estimated 37% increase in MO_2 based on PO_2 and blood flow measurements at the optic nerve head in cats.(Buerk and Riva 2002) Under hypoxia, based on the measured increase in OEF (from 0.67 to 0.74), unchanged O_{2A} (unchanged PO_{2A}), and a presumed negligible change in blood flow, the light flicker-induced MO_2 increase was estimated to be 10%. The smaller increase in MO_2 under hypoxia as compared to that under normoxia indicates systemic hypoxia suppressed the ability of MO_2 and, presumably, energy

dependent neural activity, to respond to light flicker. The estimation of a reduced MO_2 response to light flicker agrees with a previous report of attenuated electrical activity in the cat retina under a similar systemic hypoxic condition.(Kang Derwent and Linsenmeier 2000)

In conclusion, the finding of increased inner retinal OEF substantiates that inner retinal MO_2 is increased with light flicker, and that this increase may be attenuated due to limited oxygen availability under hypoxia. With impaired functional hyperemia under hypoxia, changes in OEF are expected to be dominated by alterations in MO_2 in response to light flicker. Overall, inner retinal OEF can be used for quantitative assessment of functional hyperemia with respect to the relative changes of oxygen delivery and metabolism under physiologic and pathologic conditions.

VII. RETINAL VASCULAR PO_2 LONGITUDINAL GRADIENTS

Introduction

Retinal metabolic function depends on an adequate delivery of oxygen by the chorioretinal vasculature and metabolism of oxygen by the retinal tissue. Abnormalities of oxygenation of the retinal tissue have been implicated in the development of many retinal diseases, such as retinal vascular occlusion, diabetic retinopathy, retinopathy of prematurity and glaucoma.(Arjamaa and Nikinmaa 2006; Cringle and Yu 2010; Flammer, et al. 2002; Wangsa-Wirawan and Linsenmeier 2003; Yoneya, et al. 2002) Additionally, retinal hypoxia is known to be a factor in the development of tissue damage and neovascularization.(Walshe and D'Amore 2008) Since oxygen tension (PO_2) changes in the retinal microvasculature are thought to reflect local tissue oxygen metabolism, measurements of PO_2 in and along retinal vessels may serve as useful parameters for evaluation of retinal metabolic function and understanding of local physiologic and pathologic oxygen dynamics.

Retinal tissue PO_2 across the retinal depth (Birol, et al. 2007; Cringle and Yu 2010; Wangsa-Wirawan and Linsenmeier 2003; Yu and Cringle 2001) and vascular PO_2 and oxygen saturation (SO_2) in major retinal blood vessels have been quantified previously.(Hardarson, et al. 2006; Shahidi, et al. 2009; Shonat and Kight 2003; Wilson, et al. 2005b) However, limited data have been published on the assessment of PO_2 or SO_2 longitudinal gradients along major retinal vessels,(Buerk, et al. 1993; Hardarson, et al. 2006; Shakoor, et al. 2006) and none in smaller order retinal vessels. In other tissues, while PO_2 in blood vessels of different size and radial PO_2 profiles outward from the vessel have been measured,(Intaglietta, et al. 1996; Pittman 2005; Tsai, et al. 2003) PO_2 or SO_2 longitudinal gradients along blood vessels were reported only in arterioles of the hamster's dorsal skinfold,(Torres Filho, et al. 1996) and capillaries of the rat's brain

(Vovenko 1999) and hamster's retractor muscle.(Ellsworth, et al. 1988; Stein and Ellsworth 1992)

In this chapter, a method for measurement of vascular PO_2 and gPO_2 in the retinal microvasculature of rats using three-dimensional (3D) optical section phosphorescence lifetime imaging (PLI) was demonstrated. The repeatability of vascular PO_2 and gPO_2 measurements was established and has been previously published.(Teng, et al. 2012) Measurements of gPO_2 were validated by its response to hypercapnia.

Materials and Methods

Animals

Fourteen male Long Evans pigmented rats (450 - 650 g) were used in this study. The animals were treated in compliance with the ARVO Statement for the Use of Animals in Ophthalmic and Vision Research. Rats were either ventilated with room air (21% O_2) to achieve normocapnia (N = 8) or spontaneously breathing 30% oxygen to induce elevated P_aCO_2 or hypercapnia (N = 8). Blood gas analysis was performed with a blood gas analyzer (Radiometer, Westlake, OH, USA) on arterial blood drawn from the femoral artery. Systemic arterial PO_2 (P_aO_2) in both groups of rats were maintained within the normal range (80 to 100 mmHg).(Pilbeam and Cairo 2006)

The rats were anesthetized with ketamine (100 mg/kg) and xylazine (5 mg/kg) intraperitoneally. Anesthesia was maintained by supplemental injections of ketamine (20 mg/kg) and xylazine (1 mg/kg) as needed. Pd-porphine (Frontier Scientific, Logan, UT), an oxygen sensitive molecular probe, was dissolved (12 mg/mL) in bovine serum albumin solution (60 mg/mL) and injected intravenously (20mg/kg). Body temperature

was maintained at 37ºC using an animal holder with a copper tubing water heater. The pupils were dilated with 2.5% phenylephrine and 1% tropicamide. One percent hydroxypropyl methylcellulose and a glass cover slip were applied to the cornea to eliminate the cornea's refractive power and to prevent corneal dehydration.

Instrumentation

The optical section PLI system has been described previously.(Shahidi, et al. 2009) In short, a laser beam was focused to a vertical line, and projected at an oblique angle on the retina after intravenous injection of the Pd-porphine solution. An optical section phosphorescence image of the retina was acquired with an intensified charge-coupled device camera attached to a slit lamp biomicroscope. Since the incident laser and imaging axis were not coaxial, structures at various retinal depths were laterally displaced in the section image according to depth. The laser line was scanned horizontally across the retina in small steps. For each step, a set of 10 phase delayed phosphorescence images was acquired by incrementally delaying the modulated intensifier of the imaging camera with respect to the modulated intensity of the laser beam. Imaging was performed at temporal or nasal areas within 3 disc diameters (600 μm) from the edge of the disc. During imaging, the laser power incident on the retina was approximately 40 μW, which is safe for 1 hour of continuous viewing according to the American National Standard Institute for Safety Standards.(ANSI 2007)

Image Processing and Analysis

Dedicated software algorithms were developed with Matlab (The Mathworks Inc, Natick, MA, USA) to reconstruct 3D retinal vascular PO_2 volumes from the acquired

phosphorescence section images. First, phosphorescence lifetimes and PO_2 values were obtained from the 10 phased delayed phosphorescence section images.(Lakowicz, et al. 1992; Shahidi, et al. 2009; Shonat and Kight 2003) Second, PO_2 section images were stacked contiguously to form a 3D vascular PO_2 volume with a voxel size of 8 by 8 by 10 μm^3 with no gaps or overlaps. Third, the PO_2 volume was flattened with respect to the curvature of the retina. A 3D phosphorescence volume was also generated with the same reconstruction process from the zero-phase delayed phosphorescence images.

To ensure the reliability of PO_2 measurements, voxels that did not fit well ($R^2 < 0.9$) to the theoretical relationship between phosphorescence intensity and phase delay were excluded. Exclusion of data based on fitting error is a standard method used with the phosphorescence lifetime imaging technique.(Shahidi, et al. 2009; Shonat and Johnson 1997) The remaining noise was reduced by filtering the data based on physiological validity of the calculated PO_2 values. In each animal, PO_2 measurements between 0 and the systemic P_aO_2 were included, and the mean upper tenth percentile of the feeding arterial PO_2 was used as an upper limit for PO_2 in the smaller blood vessels. Overall, 96 and 85% of the measurements were retained from large and small retinal blood vessels, respectively. As expected, a higher percentage of data were excluded from the smaller blood vessels because their size led to a lower phosphorescence signal as compared to retinal arteries and veins.

The retinal vessels were segmented based on the semi-automated as proposed in Chapter IV using the phosphorescence volume. In brief, for each vessel, a 3D binary volume was generated by manual segmentation. Along each blood vessel, upstream and downstream locations were manually selected based on the extent of the imaged retinal area, which was contingent upon the curvature of the eye and dilation of the pupil. A centerline along the vessel was identified using distance transformations (Borgefors

1996; Zhou and Toga 1999) between vessel upstream and downstream locations. The centerline was then smoothed with cubic smoothing spline functions,(De Boor 2001) resulting in an average distance of 7 μm between centerline points. For visualizing three dimensional volumes, images were rendered with Paraview software.(Kitware Inc, Clifton Park, NY, USA).

From the PO_2 volumes generated in each rat, 3 types of blood vessels were selected consisting of a major retinal artery and vein pair, and a smaller blood vessel (microvessel) between them. These microvessels had diameters less than half of the major blood vessels, and had lengths of 100 μm or more.

Data Analysis and Statistics

A mean PO_2 (mPO_2) was calculated in each blood vessel by averaging PO_2 measurements over the segmented vessel. PO_2 at each centerline point along the vessel was calculated by averaging PO_2 over a cross-sectional area perpendicular to the centerline. Linear regression analysis was performed on PO_2 measurements along the vessel centerline and the slope of the best fit line was defined as PO_2 longitudinal gradient (gPO_2).

Reproducibility of measurements was assessed by determining intraclass correlation coefficient (ICC) and absolute difference between 2 repeated measurements in 8 sets of vessels. Two-way analysis of variance (Pinheiro, et al. 2007) was performed to determine the effects of P_aCO_2 (as between subject factor) and vessel type (as within subject factor) on mPO_2 and gPO_2. Post hoc pair-wise comparisons (Bonferroni) were performed to determine measurement differences between vessel types and the effect of hypercapnia within each vessel type. Statistical significance was accepted at $P < 0.05$.

Results

Systemic Physiologic Status

Systemic arterial P_aO_2, P_aCO_2 and blood pH measurements in rats under normocapnia and hypercapnia are shown in Table VI. As expected, the hypercapnic group had a significantly higher P_aCO_2 as compared to that in the normocapnic group. Consequently, the arterial pH in the hypercapnic group was lower as compared to that in the normocapnic group (P = 0.01). The means of P_aO_2 between the two groups were not statistically different (P = 0.55).

TABLE VI MEAN SYSTEMIC PHYSIOLOGICAL PARAMETERS IN NORMOMCAPNIC AND HYPERCAPNIC GROUPS.

	P_aO_2	P_aCO_2	pH
Normocapnia (N = 8)	89 ± 7	39 ± 7	7.39±0.04
Hypercapnia (N = 8)	91 ± 5	62 ±10	7.29±0.06
P-value	0.55	<0.01	0.01

Reproducibility

Mean PO_2 measurements in arteries, microvessels and veins were reproducible (ICC > 0.86; p < 0.01; N = 8). Mean absolute differences of mPO_2 in arteries, microvessels and veins were 1.5, 3.1 and 1.2 mmHg (N = 8), respectively. PO_2 gradient measurements in retinal microvessel and veins were reproducible (ICC > 0.88; p < 0.01;

N = 8). Mean absolute differences of gPO_2 in microvessels and veins were 0.56 and 0.29 mmHg/100µm, respectively. The ICC of gPO_2 measurements in retinal arteries was relatively low (ICC = 0.58; p = 0.04; N = 8), therefore retinal arterial gPO_2 measurements were excluded from further analysis.

Vascular PO_2

An example of a 3D phosphorescence volume obtained in one rat is shown in Fig 19a. Vessel segmentations and centerlines of a microvessel and vein are displayed in Fig 19b. The segmented vascular PO_2 volume is shown in Fig 19c.

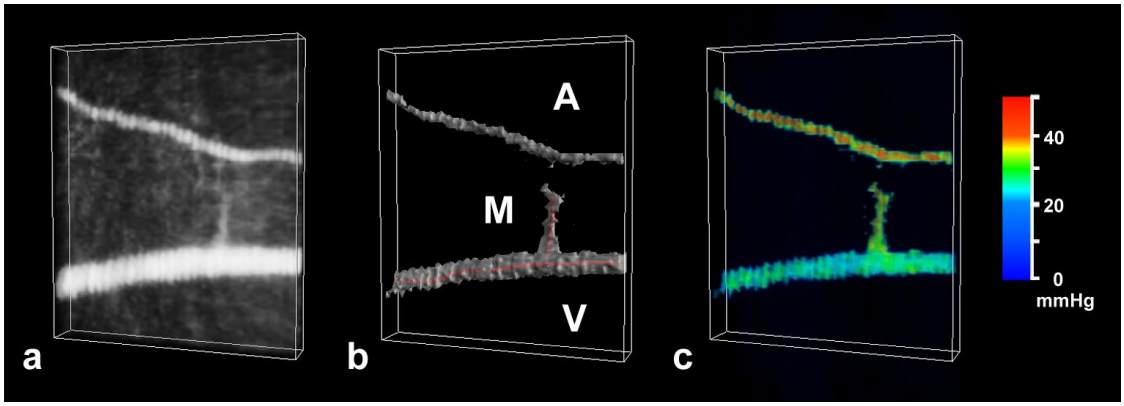

Fig. 19 (a) An example of a three dimensional phosphorescence volume of the retinal microvasculature in one rat. (b) Segmented artery (A), microvessel (M) and vein (V) and their corresponding centerlines (red solid lines). (c) Segmented vascular PO2 volume; color bar shows PO2 measurements in mmHg. Figure reprinted from Teng, et al.(Teng, et al. 2012)

Mean mPO_2 measurements in retinal arteries, microvessels and veins under normocapnia and hypercapnia are shown in Fig. 20. Under normocapnia, mean mPO_2 in arteries, microvessels and veins were 39 ± 6, 30 ± 4 and 20 ± 4 mmHg, respectively. While under hypercapnia, mean mPO_2 in arteries, microvessels and veins were 38 ± 6, 31 ± 6 and 27 ± 4 mmHg, respectively. The effect of vessel type on mPO_2 was significant ($P < 0.01$), while the effect of P_aCO_2 on mPO_2 was insignificant ($P = 0.38$).

However, there was a significant interaction effect between vessel type and $PaCO_2$ ($P < 0.01$), and as a result post hoc pair-wise comparisons were performed. Under both normocapnia and hypercapnia, mean mPO_2 of arteries was significantly higher than those of microvessels and veins ($P < 0.01$). Similarly, mean microvessel mPO_2 was significantly higher than those in veins ($P < 0.01$) under both normocapnia and hypercapnia. The effect of P_aCO_2 was only significant on venous mPO_2, under hypercapnia, venous mPO_2 was higher than that under normocapnia ($P = 0.02$).

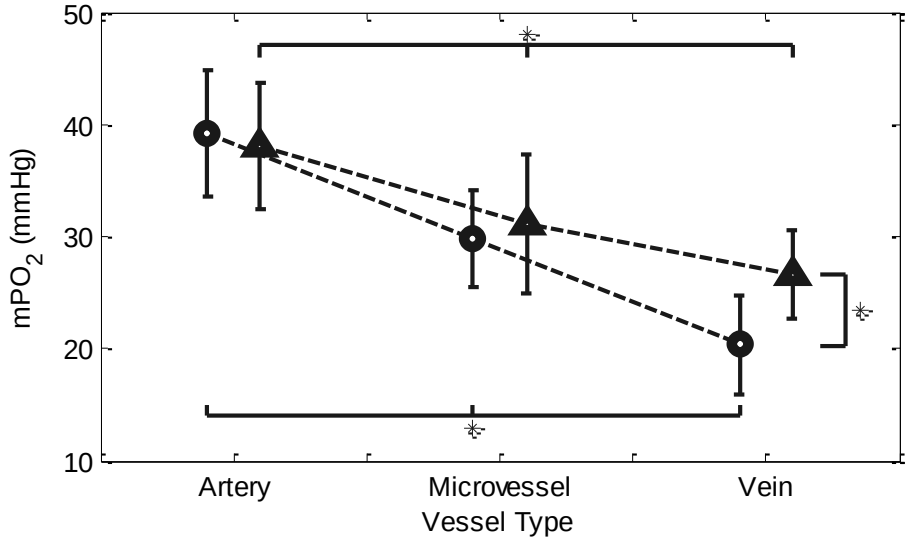

Fig. 20 Measurements of mPO2 (Mean ± SD bar) in retinal arteries, microvessels and veins under normocapnia (O) and hypercapnia (Δ). The effect of vessel type on mPO2 was significant (P < 0.01), while the effect of PaCO2 on mPO2 was insignificant (P = 0.38). However, there was a significant interaction effect between vessel type and PaCO2 (P < 0.01). Asterisks indicate significant pair-wise differences (P < 0.01) observed based on the post hoc comparisons.

PO_2 Longitudinal Gradients

An example of PO_2 measurements as a function of distance along a retinal microvessel is shown in Fig. 21. The slope of the best fit line to the PO_2 measurements (gPO_2) was -3.65 mmHg/100µm. Mean gPO_2 measurements are shown in Fig 22.

Under normocapnia, mean gPO_2 in microvessels and veins were -5.0 ± 1.0 and 0.0 ± 0.5 mmHg/100µm, respectively. While under hypercapnia, mean gPO_2 in microvessels and veins were -3.6 ± 0.8 and -0.2 ± 0.4 mmHg/100µm, respectively. The effect of vessel type on gPO_2 was significant ($P < 0.01$), while the effect of P_aCO_2 on gPO_2 was insignificant ($P = 0.06$). However, there was a significant interaction effect between vessel type and P_aCO_2 ($P = 0.01$). Based on the pair-wise post hoc comparisons, under both normocapnia and hypercapnia, mean gPO_2 measurements in microvessels were significantly steeper (more negative) than those in veins ($P < 0.01$). The effect of $PaCO_2$ was significant on microvessel gPO_2; where under hypercapnia, microvessel gPO_2 was less steep than that under normocapnia ($P = 0.01$).

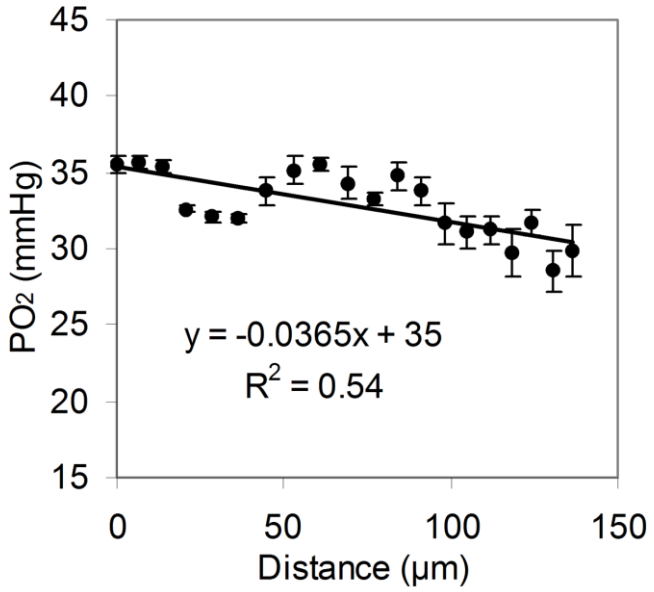

Fig. 21 PO2 measurements plotted as a function of distance along a retinal microvessel in one rat. The best fit regression line and corresponding linear equation are displayed. Error bars represent standard errors of the means of 6 to 12 measurements. Figure reprinted from Teng, et al.(Teng, et al. 2012)

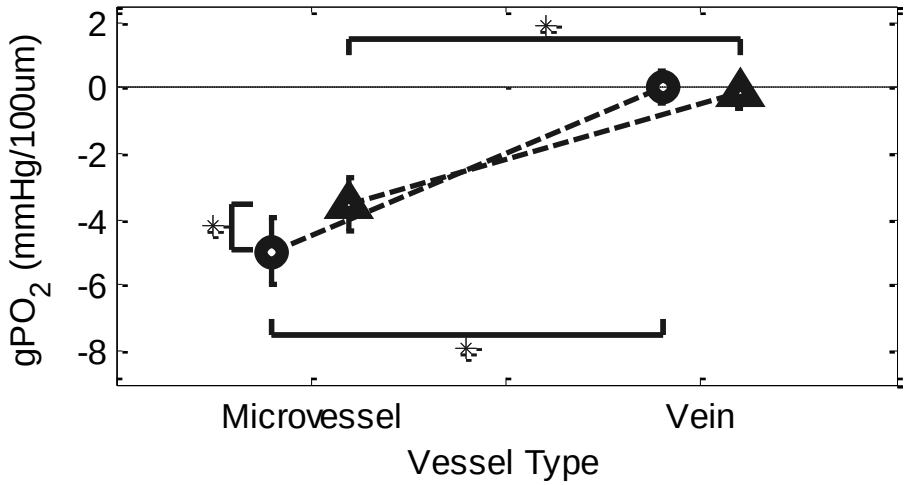

Fig. 22 Measurements of gPO_2 (Mean ± SD bar) in retinal microvessels and veins under normocapnia (O) and hypercapnia (Δ). The effect of vessel type on gPO_2 was significant (P<0.01), while the effect of $PaCO_2$ on gPO_2 was insignificant (P=0.06). However, there was a significant interaction between vessel type and $PaCO_2$ (P=0.01). Asterisks indicate significant pair-wise differences (P ≤ 0.01) observed based on the post hoc comparisons. Dashed line indicates a gPO_2 of 0 mmHg/100μm.

Discussion

Longitudinal changes in PO_2 along retinal blood vessels are indicative of retinal tissue oxygen extraction and are expected to be related to the retinal metabolic function. In this chapter, a method for measuring mPO_2 and gPO_2 in retinal arteries, microvessels and veins of rats was established. This is the first study to report quantitative and reproducible measurements of PO_2 in retinal blood vessels that are approximately 20 μm in diameter.

In the current study, microvessel gPO_2 measurements were negative under both normocapnic and hypercapnic conditions. The negative gPO_2 obtained in these microvessels are in agreement with the progressively reduced mPO_2 measured in the retinal arteries, microvessels and veins, indicative of oxygen extraction by the tissue across the retinal microvasculature. Furthermore, although retinal capillaries are

commonly thought to be the primary site for oxygen delivery, the substantial oxygen loss along the observed retinal microvessels indicates oxygen extraction by the retinal tissue occurs not only at the capillary level. PO_2 measurements in retinal arteries were more variable because of the lower sensitivity of the Pd-porphine dye at high PO_2.(Shonat and Kight 2003) This variability coupled with the presumed small change in PO_2 along retinal arteries,(Buerk, et al. 1993; Liu, et al. 2009) limited measurements of retinal arterial gPO_2. The magnitude of retinal venous gPO_2 was relatively small and its sign was variable. This finding concurs with reported oxygen flux measurements in the vitreous of cats, showing the direction of oxygen flux to be either going inward or outward from the veins.(Buerk, et al. 1993) Additionally, diffusional shunting directly from retinal arteries to veins may also contribute to variations in venous gPO_2.(Riva, et al. 1986)

Validation of the gPO_2 measurements was carried out by measuring the response of gPO_2 to hypercapnia. Since hypercapnia has been shown to increase retinal blood flow,(Harris, et al. 1995; Venkataraman, et al. 2008) according to Fick's principle,(Boulpaep 2005) gPO_2 is expected to decrease (less negative) assuming a minimal change in oxygen metabolism as found in the brain.(Chen and Pike 2010; Davis, et al. 1998; Jain, et al. 2011; Kim, et al. 1999; Stefanovic, et al. 2004) As expected, mean microvessel gPO_2 under hypercapnia was significantly less negative as compared to that under normocapnia. Furthermore, the downstream venous mPO_2 correspondingly increased, which further validates the observed effect of hypercapnia on gPO_2. On the contrary, the effect of hypercapnia on venous gPO_2 was found to be insignificant. Since diffusion of oxygen between the vessel and tissue occurs regardless of vessel types,(Buerk, et al. 1993; Tsai, et al. 2003) the effect of hypercapnia on both microvessel and venous gPO_2 should be similar. However, the relatively small

magnitude of venous gPO_2 likely hindered the ability of the current method to detect a significant hypercapnic effect on venous gPO_2.

In summary, a method for quantitative measurements of mPO_2 and gPO_2 in retinal microvasculature of rats was established. The steepness of the retinal microvessel gPO_2 indicates substantial oxygen loss along their lengths, similar to the expected oxygen loss from retinal capillaries. Since the retinal capillary network is anastomotic, its branching and ensuing short vessel segments hinders reliable quantification of gPO_2 by any existing technique. Therefore, retinal microvessels may serve as a valuable surrogate for studying retinal oxygen transport. In future studies, 3D PO_2 imaging of multiple retinal areas to increase the microvessel sample size will allow a comprehensive assessment of retinal oxygen dynamics in response to physiological challenges or pathological conditions.

CITED LITERATURE

Ahmed, J., R. A. Linsenmeier, and R. Dunn, Jr.
1994 The oxygen distribution in the prelaminar optic nerve head of the cat. Exp Eye Res 59(4):457-65.

Ahmed, J., M. K. Pulfer, and R. A. Linsenmeier
2001 Measurement of blood flow through the retinal circulation of the cat during normoxia and hypoxemia using fluorescent microspheres. Microvasc Res 62(2):143-53.

Alperin, N., and S. H. Lee
2003 PUBS: pulsatility-based segmentation of lumens conducting non-steady flow. Magn Reson Med 49(5):934-44.

Altman, D. G., and J. M. Bland
1983 Measurement in Medicine - the Analysis of Method Comparison Studies. Statistician 32(3):307-317.

Anand-Apte, B.
Hollyfield, J.G.
2011 Developmental Anatomy of the Retinal and Choroidal Vasculature. *In* Immunology, Inflammation and Diseases of the Eye. D.A. Dartt, R. Dana, P. D'Amore, and J. Niederkorn, eds. Pp. 186-192. San Diego, CA: Academic Press.

Anderson, B., Jr.
1968 Ocular effects of changes in oxygen and carbon dioxide tension. Trans Am Ophthalmol Soc 66:423-74.

ANSI
2007 American National Standard for Safe Use of Lasers ANSI Z136.1-2007. Orlando, FL: Laser Institute of America.

Arjamaa, O., and M. Nikinmaa
2006 Oxygen-dependent diseases in the retina: role of hypoxia-inducible factors. Experimental eye research 83(3):473-483.

Bankhead, P., et al.
2012 Fast retinal vessel detection and measurement using wavelets and edge location refinement. PLoS One 7(3):e32435.

Baron, J. C., and T. Jones
2012 Oxygen metabolism, oxygen extraction and positron emission tomography: Historical perspective and impact on basic and clinical neuroscience. Neuroimage 61(2):492-504.

Beach, J. M., et al.
1999 Oximetry of retinal vessels by dual-wavelength imaging: calibration and influence of pigmentation. J Appl Physiol (1985) 86(2):748-58.

Beach, J., J. Ning, and B. Khoobehi
2007 Oxygen saturation in optic nerve head structures by hyperspectral image analysis. Curr Eye Res 32(2):161-70.

Bek, T., J. Hajari, and P. Jeppesen
2008 Interaction between flicker-induced vasodilatation and pressure autoregulation in early retinopathy of type 2 diabetes. Graefes Arch Clin Exp Ophthalmol 246(5):763-9.

Bill, A., and G. O. Sperber
1990 Aspects of oxygen and glucose consumption in the retina: effects of high intraocular pressure and light. Graefes Arch Clin Exp Ophthalmol 228(2):124-7.

Birol, G., et al.
2007 Oxygen distribution and consumption in the macaque retina. American journal of physiology.Heart and circulatory physiology 293(3):H1696-H1704.

Blair, N. P., et al.
2009 Abnormal retinal vascular oxygen tension response to light flicker in diabetic rats. Invest Ophthalmol Vis Sci 50(11):5444-8.

Borgefors, G.
1986 Distance transformations in digital images. Computer Vision, Graphics, and Image Processing 34(3):344-371.

Borgefors, G.
1996 On Digital Distance Transforms in Three Dimensions. Computer Vision and Image Understanding 64(3):368-376.

Boron, W. F., and E. L. Boulpaep
2005 Medical Physiology. Philadelphia, PA: Elsevier Saunders.

Boulpaep, E. L.

2005 Organization of the Cardiovascular System. *In* Medical physiology. W.F. Boron and E.L. Boulpaep, eds. Pp. 423-446. Philadelphia, Pennsylvania, USA: Elsevier Saunders.

Braun, R. D., R. A. Linsenmeier, and T. K. Goldstick
1995 Oxygen consumption in the inner and outer retina of the cat. Invest Ophthalmol Vis Sci 36(3):542-54.

Braun, R. D., R. A. Linsenmeier, and C. M. Yancey
1992 Spontaneous fluctuations in oxygen tension in the cat retina. Microvasc Res 44(1):73-84.

Buerk, D. G., D. N. Atochin, and C. E. Riva
1998 Simultaneous tissue PO2, nitric oxide, and laser Doppler blood flow measurements during neuronal activation of optic nerve. Adv Exp Med Biol 454:159-64.

Buerk, D. G., and C. E. Riva
2002 Adenosine enhances functional activation of blood flow in cat optic nerve head during photic stimulation independently from nitric oxide. Microvasc Res 64(2):254-64.

Buerk, D. G., et al.
1993 O2 gradients and countercurrent exchange in the cat vitreous humor near retinal arterioles and venules. Microvascular research 45(2):134-148.

Cartheuser, C. F.
1993 Standard and pH-affected hemoglobin-O2 binding curves of Sprague-Dawley rats under normal and shifted P50 conditions. Comp Biochem Physiol Comp Physiol 106(4):775-82.

Chen, J., A. Edwards, and A. T. Layton
2010 Effects of pH and medullary blood flow on oxygen transport and sodium reabsorption in the rat outer medulla. Am J Physiol Renal Physiol 298(6):F1369-F1383.

Chen, J. J., and G. B. Pike
2010 Global cerebral oxidative metabolism during hypercapnia and hypocapnia in humans: implications for BOLD fMRI. J Cereb Blood Flow Metab 30(6):1094-9.

Connor, K. M., et al.

2009 Quantification of oxygen-induced retinopathy in the mouse: a model of vessel loss, vessel regrowth and pathological angiogenesis. Nat Protoc 4(11):1565-73.

Cringle, S. J., and D. Y. Yu
2010 Oxygen supply and consumption in the retina: implications for studies of retinopathy of prematurity. Documenta ophthalmologica. Advances in ophthalmology 120(1):99-109.

Crystal, G.J.
2001 Principles of cardiovascular physiology. *In* Cardiac anesthesia: principles and clinical practice. F.G. Estafanous, P.G. Barash, and J.G. Reves, eds. Pp. 37-57. Philadelphia, PA: Lippincott Williams & Wilkins.

Davis, M.J., M.A. Hill, and L. Kuo
2008 Local regulation of microvascular perfusion. *In* Microcirculation. R.F. Tuma, W.N. Duran, and K. Ley, eds. Pp. 161–284. Sandiego, CA: Academic Press.

Davis, T. L., et al.
1998 Calibrated functional MRI: mapping the dynamics of oxidative metabolism. Proc Natl Acad Sci U S A 95(4):1834-9.

De Boor, C.
2001 Smoothing and least-squares approximation. *In* A practical guide to splines. C. De Boor, ed. Pp. 207-210. New York, NY: Springer.

Delori, F. C.
1988 Noninvasive technique for oximetry of blood in retinal vessels. Appl Opt 27(6):1113-25.

Derdeyn, C. P.
2007 Pet Imaging in Carotid Stenosis. *In* Imaging of carotid artery stenosis. B. Schaller, ed. Pp. 85-102. New York: Springer.

Derdeyn, C. P., R. L. Grubb, Jr., and W. J. Powers
1999 Cerebral hemodynamic impairment: methods of measurement and association with stroke risk. Neurology 53(2):251-259.

Durukan, A., and T. Tatlisumak
2007 Acute ischemic stroke: overview of major experimental rodent models, pathophysiology, and therapy of focal cerebral ischemia. Pharmacol Biochem Behav 87(1):179-97.

Ellsworth, M. L., A. S. Popel, and R. N. Pittman
1988 Assessment and impact of heterogeneities of convective oxygen transport parameters in capillaries of striated muscle: experimental and theoretical. Microvascular research 35(3):341-362.

Eysteinsson, T., et al.
2014 Retinal vessel oxygen saturation and vessel diameter in retinitis pigmentosa. Acta Ophthalmol.

Fisher, M.
1997 Characterizing the target of acute stroke therapy. Stroke 28(4):866-72.

Flammer, J., et al.
2002 The impact of ocular blood flow in glaucoma. Progress in retinal and eye research 21(4):359-393.

Fraz, M. M., et al.
2012 Blood vessel segmentation methodologies in retinal images--a survey. Comput Methods Programs Biomed 108(1):407-33.

Garhofer, G., et al.
2004a Response of retinal vessel diameters to flicker stimulation in patients with early open angle glaucoma. J Glaucoma 13(4):340-4.

Garhofer, G., et al.
2004b Reduced response of retinal vessel diameters to flicker stimulation in patients with diabetes. Br J Ophthalmol 88(7):887-91.

Geirsdottir, A., et al.
2014 Retinal oxygen metabolism in exudative age-related macular degeneration. Acta Ophthalmol 92(1):27-33.

Geirsdottir, A., et al.
2012 Retinal vessel oxygen saturation in healthy individuals. Invest Ophthalmol Vis Sci 53(9):5433-42.

Gibbs, E. L., et al.
1942 Arterial and cerebral venous blood: arterial-venous differences in man. J Biol Chem 144:325-332.

Grubb, R. L., Jr., et al.

1998 Importance of hemodynamic factors in the prognosis of symptomatic carotid occlusion. JAMA 280(12):1055-60.

Hammer, M., et al.
2012 Retinal Vessel Oxygen Saturation under Flicker Light Stimulation in Patients with Non-Proliferative Diabetic Retinopathy. Invest Ophthalmol Vis Sci.

Hammer, M., et al.
2001 Light paths in retinal vessel oxymetry. IEEE Trans Biomed Eng 48(5):592-8.

Hammer, M., E. Thamm, and D. Schweitzer
2002 A simple algorithm for in vivo ocular fundus oximetry compensating for non-haemoglobin absorption and scattering. Physics in Medicine and Biology 47(17):N233-8.

Hammer, M., et al.
2011 Retinal venous oxygen saturation increases by flicker light stimulation. Invest Ophthalmol Vis Sci 52(1):274-7.

Hammer, M., et al.
2009 Diabetic patients with retinopathy show increased retinal venous oxygen saturation. Graefe's archive for clinical and experimental ophthalmology = Albrecht von Graefes Archiv fur klinische und experimentelle Ophthalmologie 247(8):1025-30.

Hammer, M., et al.
2008 Retinal vessel oximetry-calibration, compensation for vessel diameter and fundus pigmentation, and reproducibility. Journal of Biomedical Optics 13(5).

Hardarson, S. H.
2013 Retinal oximetry. Acta Ophthalmol 91(5):489-90.

Hardarson, S. H., et al.
2009 Oxygen saturation in human retinal vessels is higher in dark than in light. Invest Ophthalmol Vis Sci 50(5):2308-11.

Hardarson, S. H., et al.
2013 Retinal oximetry in central retinal artery occlusion. Acta Ophthalmol 91(2):189-90.

Hardarson, S. H., et al.

2006 Automatic retinal oximetry. Invest Ophthalmol Vis Sci 47(11):5011-6.

Hardarson, S. H., and E. Stefansson
2010 Oxygen saturation in central retinal vein occlusion. Am J Ophthalmol 150(6):871-5.

Hardarson, S. H., and E. Stefansson
2012 Retinal oxygen saturation is altered in diabetic retinopathy. Br J Ophthalmol 96(4):560-3.

Harper, A. M., and R. A. Bell
1963 The Effect of Metabolic Acidosis and Alkalosis on the Blood Flow through the Cerebral Cortex. J Neurol Neurosurg Psychiatry 26:341-4.

Harris, A., et al.
1995 CO2 dependence of retinal arterial and capillary blood velocity. Acta Ophthalmologica Scandinavica 73(5):421-424.

Hayreh, S. S.
2011 Acute retinal arterial occlusive disorders. Prog Retin Eye Res 30(5):359-94.

Hayreh, S. S., and T. A. Weingeist
1980 Experimental occlusion of the central artery of the retina. IV: Retinal tolerance time to acute ischaemia. Br J Ophthalmol 64(11):818-25.

Hayreh, S. S., et al.
2004 Central retinal artery occlusion. Retinal survival time. Exp Eye Res 78(3):723-36.

Heiss, W. D., et al.
1998 Quantitative neuroimaging for the evaluation of the effect of stroke treatment. Cerebrovasc Dis 8 Suppl 2:23-9.

Heiss, W. D., and K. Herholz
1994 Assessment of pathophysiology of stroke by positron emission tomography. Eur J Nucl Med 21(5):455-65.

Hermansen, M. C., U. R. Kotagal, and L. I. Kleinman
1984 The effect of metabolic acidosis upon autoregulation of cerebral blood flow in newborn dogs. Brain Res 324(1):101-5.

Hickam, J. B., R. Frayser, and J. C. Ross
1963 A study of retinal venous blood oxygen saturation in human subjects by photographic means. Circulation 27:375-85.

Hoffman, W. E., R. F. Albrecht, and D. J. Miletich
1984 Cerebrovascular response to hypoxia in young vs aged rats. Stroke 15(1):129-33.

Intaglietta, M., P. C. Johnson, and R. M. Winslow
1996 Microvascular and tissue oxygen distribution. Cardiovasc Res 32(4):632-43.

Ito, H., et al.
2004 Database of normal human cerebral blood flow, cerebral blood volume, cerebral oxygen extraction fraction and cerebral metabolic rate of oxygen measured by positron emission tomography with 15O-labelled carbon dioxide or water, carbon monoxide and oxygen: a multicentre study in Japan. Eur J Nucl Med Mol Imaging 31(5):635-43.

Ito, Y., and B. A. Berkowitz
2001 MR studies of retinal oxygenation. Vision Res 41(10-11):1307-11.

Jaime, G. R., et al.
2012 Acute variations in retinal vascular oxygen content in a rabbit model of retinal venous occlusion. PLoS One 7(11):e50179.

Jain, V., et al.
2011 Rapid magnetic resonance measurement of global cerebral metabolic rate of oxygen consumption in humans during rest and hypercapnia. J Cereb Blood Flow Metab 31(7):1504-12.

Jani, P. D., et al.
2014 Normative values and predictors of retinal oxygen saturation. Retina 34(2):394-401.

Johannsson, H., and B. K. Siesjo
1975 Cerebral blood flow and oxygen consumption in the rat in hypoxic hypoxia. Acta Physiol Scand 93(2):269-76.

Jorgensen, C. M., S. H. Hardarson, and T. Bek
2014 The oxygen saturation in retinal vessels from diabetic patients depends on the severity and type of vision-threatening retinopathy. Acta Ophthalmol 92(1):34-9.

Kang Derwent, J., and R. A. Linsenmeier
2000 Effects of hypoxemia on the a- and b-waves of the electroretinogram in the cat retina. Invest Ophthalmol Vis Sci 41(11):3634-42.

Khoobehi, B., et al.
2013 Retinal arterial and venous oxygen saturation is altered in diabetic patients. Invest Ophthalmol Vis Sci 54(10):7103-6.

Kim, S. G., et al.
1999 Determination of relative CMRO2 from CBF and BOLD changes: significant increase of oxygen consumption rate during visual stimulation. Magn Reson Med 41(6):1152-61.

Kirbas, C., and F. Quek
2004 A review of vessel extraction techniques and algorithms. ACM Computing Surveys 36(2):81-121.

Kobayashi, M., et al.
2012 Cerebral oxygen metabolism of rats using injectable (15)O-oxygen with a steady-state method. J Cereb Blood Flow Metab 32(1):33-40.

Kur, J., E. A. Newman, and T. Chan-Ling
2012 Cellular and physiological mechanisms underlying blood flow regulation in the retina and choroid in health and disease. Prog Retin Eye Res 31(5):377-406.

Lakowicz, J. R., et al.
1992 Fluorescence lifetime imaging. Anal Biochem 202(2):316-30.

Lasta, M., et al.
2013 Neurovascular dysfunction precedes neural dysfunction in the retina of patients with type 1 diabetes. Invest Ophthalmol Vis Sci 54(1):842-7.

Lau, J. C., and R. A. Linsenmeier
2012 Oxygen consumption and distribution in the Long-Evans rat retina. Exp Eye Res 102:50-8.

Linsenmeier, R. A.
1990 Electrophysiological consequences of retinal hypoxia. Graefes Arch Clin Exp Ophthalmol 228(2):143-50.

Linsenmeier, R. A.

2012 Oxygen Measurements in Animals. *In* Ocular Blood Flow. L. Schmetterer and J. Kiel, eds. Pp. 65-93. Heidelberg Springer-Verlag.

Linsenmeier, R. A., and R. D. Braun
1992 Oxygen distribution and consumption in the cat retina during normoxia and hypoxemia. J Gen Physiol 99(2):177-97.

Linsenmeier, R. A., et al.
1998 Retinal hypoxia in long-term diabetic cats. Investigative Ophthalmology & Visual Science 39(9):1647-1657.

Liu, D., et al.
2009 Computational analysis of oxygen transport in the retinal arterial network. Current eye research 34(11):945-956.

Lo, L. W., C. J. Koch, and D. F. Wilson
1996 Calibration of oxygen-dependent quenching of the phosphorescence of Pd-meso-tetra (4-carboxyphenyl) porphine: a phosphor with general application for measuring oxygen concentration in biological systems. Anal Biochem 236(1):153-60.

Magata, Y., et al.
2003 Development of injectable O-15 oxygen and estimation of rat OEF. J Cereb Blood Flow Metab 23(6):671-6.

McLeod, D.
2012 Letter to the editor: partial central retinal artery occlusion offers a unique insight into the ischemic penumbra. Clin Ophthalmol 6:9-22.

McPherson, R. W., S. Zeger, and R. J. Traystman
1986 Relationship of somatosensory evoked potentials and cerebral oxygen consumption during hypoxic hypoxia in dogs. Stroke 17(1):30-6.

Mezu-Ndubuisi, O. J., et al.
2013 In vivo retinal vascular oxygen tension imaging and fluorescein angiography in the mouse model of oxygen-induced retinopathy. Invest Ophthalmol Vis Sci 54(10):6968-72.

Muir, K. W., et al.
2006 Imaging of acute stroke. Lancet Neurol 5(9):755-68.

Nagaoka, T., et al.

2002 The effect of nitric oxide on retinal blood flow during hypoxia in cats. Invest Ophthalmol Vis Sci 43(9):3037-44.

National Eye Institute, NIH
2014 Retina, Vol. 2014: Wikipedia, Contributors.

Newman, E. A.
2013 Functional hyperemia and mechanisms of neurovascular coupling in the retinal vasculature. J Cereb Blood Flow Metab.

Olafsdottir, O. B., et al.
2011 Retinal oximetry in primary open-angle glaucoma. Invest Ophthalmol Vis Sci 52(9):6409-13.

Olafsdottir, O. B., et al.
2014 Retinal oxygen metabolism in healthy subjects and glaucoma patients. Br J Ophthalmol.

Osborne, N. N., et al.
2004 Retinal ischemia: mechanisms of damage and potential therapeutic strategies. Prog Retin Eye Res 23(1):91-147.

Oshima, T., F. Karasawa, and T. Satoh
2002 Effects of propofol on cerebral blood flow and the metabolic rate of oxygen in humans. Acta Anaesthesiol Scand 46(7):831-5.

Otsu, Nobuyuki
1975 A threshold selection method from gray-level histograms. Automatica 11(285-296):23-27.

Padnick, L. B., R. A. Linsenmeier, and T. K. Goldstick
1999 Oxygenation of the cat primary visual cortex. J Appl Physiol (1985) 86(5):1490-6.

Palsson, O., et al.
2012 Retinal oximetry images must be standardized: a methodological analysis. Invest Ophthalmol Vis Sci 53(4):1729-33.

Pilbeam, Susan P., and Jimmy M. Cairo
2006 Mechanical ventilation : physiological and clinical applications. St. Louis: Mosby Elsevier.

Pinheiro, Jose, et al.
2007 Linear and nonlinear mixed effects models. R package version 3:57.

Pittman, R. N.
2005 Oxygen transport and exchange in the microcirculation. Microcirculation 12(1):59-70.

Pittman, R. N.
2011 Oxygen Transport in Normal and Pathological Situations: Defects and Compensations. *In* Regulation of Tissue Oxygenation. R.N. Pittman, ed. Pp. 47-50. San Rafael, CA: Morgan & Claypool Life Sciences.

Pournaras, C. J., et al.
2008 Regulation of retinal blood flow in health and disease. Prog Retin Eye Res 27(3):284-330.

Powers, W. J.
2012 Stroke: Misery perfusion in cerebrovascular disease-is it important? Nat Rev Neurol 8(9):479-80.

Powers, W. J., and A. R. Zazulia
2010 PET in Cerebrovascular Disease. PET Clin 5(1):83106.

Riva, C. E.
1998 Noninvasive measurement of oxygen tension in the optic nerve head. Curr Opin Ophthalmol 9(2):56-60.

Riva, C. E., E. Logean, and B. Falsini
2005 Visually evoked hemodynamical response and assessment of neurovascular coupling in the optic nerve and retina. Prog Retin Eye Res 24(2):183-215.

Riva, C. E., C. J. Pournaras, and M. Tsacopoulos
1986 Regulation of local oxygen tension and blood flow in the inner retina during hyperoxia. Journal of applied physiology (Bethesda, Md.: 1985) 61(2):592-598.

Riva, C. E., et al.
2004 Flicker-evoked response measured at the optic disc rim is reduced in ocular hypertension and early glaucoma. Invest Ophthalmol Vis Sci 45(10):3662-8.

Sakadzic, S., et al.
2010 Two-photon high-resolution measurement of partial pressure of oxygen in cerebral vasculature and tissue. Nat Methods 7(9):755-9.

Shahidi, M., et al.
2006 A method for chorioretinal oxygen tension measurement. Curr Eye Res 31(4):357-66.

Shahidi, M., et al.
2010 Retinal tissue oxygen tension imaging in the rat. Invest Ophthalmol Vis Sci 51(9):4766-70.

Shahidi, M., et al.
2009 Three-dimensional mapping of chorioretinal vascular oxygen tension in the rat. Invest Ophthalmol Vis Sci 50(2):820-5.

Shakoor, A., et al.
2006 Chorioretinal vascular oxygen tension changes in response to light flicker. Investigative ophthalmology & visual science 47(11):4962-4965.

Shih, Y. Y., et al.
2011 Lamina-specific functional MRI of retinal and choroidal responses to visual stimuli. Invest Ophthalmol Vis Sci 52(8):5303-10.

Shih, Y. Y., et al.
2013 Quantitative retinal and choroidal blood flow during light, dark adaptation and flicker light stimulation in rats using fluorescent microspheres. Curr Eye Res 38(2):292-8.

Shonat, R. D., and P. C. Johnson
1997 Oxygen tension gradients and heterogeneity in venous microcirculation: a phosphorescence quenching study. American Journal of Physiology- Heart and Circulatory Physiology 272(5):H2233-H2240.

Shonat, R. D., and A. C. Kight
2003 Oxygen tension imaging in the mouse retina. Ann Biomed Eng 31(9):1084-96.

Staal, J., et al.
2004 Ridge-based vessel segmentation in color images of the retina. IEEE Trans Med Imaging 23(4):501-9.

Stefanovic, B., J. M. Warnking, and G. B. Pike
2004 Hemodynamic and metabolic responses to neuronal inhibition. Neuroimage 22(2):771-8.

Stein, J. C., and M. L. Ellsworth
1992 Microvascular oxygen transport: impact of a left-shifted dissociation curve. American Journal of Physiology- Heart and Circulatory Physiology 262(2):H517-H522.

Strenn, K., et al.
1997 Reproducibility and sensitivity of scanning laser Doppler flowmetry during graded changes in PO2. Br J Ophthalmol 81(5):360-4.

Sun, Y., and D. L. Parker
1999 Performance analysis of maximum intensity projection algorithm for display of MRA images. IEEE Transactions on Medical Imaging 18(12):1154-1169.

Suri, J. S., et al.
2002 A review on MR vascular image processing: skeleton versus nonskeleton approaches: part II. IEEE Transactions on Information Technology in Biomedicine 6(4):338-350.

Takahashi, G. H., I. Fatt, and T. K. Goldstick
1966 Oxygen consumption rate of tissue measured by a micropolarographic method. J Gen Physiol 50(2):317-35.

Teng, P. Y., A. M. Bagci, and N. Alperin
2011 Automated prescription of an optimal imaging plane for measurement of cerebral blood flow by phase contrast magnetic resonance imaging. IEEE Trans Biomed Eng 58(9):2566-73.

Teng, P. Y., et al.
2012 Oxygen tension and gradient measurements in the retinal microvasculature of rats. Graefes Arch Clin Exp Ophthalmol 250(3):361-7.

Teng, P. Y., et al.
2013 Inner retinal oxygen extraction fraction in rat. Invest Ophthalmol Vis Sci 54(1):647-51.

Torres Filho, I. P., H. Kerger, and M. Intaglietta
1996 pO2 measurements in arteriolar networks. Microvasc Res 51(2):202-212.

Traustason, S., et al.
2011 Retinal oxygen saturation in patients with systemic hypoxemia. Invest Ophthalmol Vis Sci 52(8):5064-7.

Traustason, S., et al.
2013 Spectrophotometric retinal oximetry in pigs. Invest Ophthalmol Vis Sci 54(4):2746-51.

Traustason, S., M. la Cour, and M. Larsen
2014 Retinal vascular oximetry during ranibizumab treatment of central retinal vein occlusion. Br J Ophthalmol.

Tsai, A. G., P. C. Johnson, and M. Intaglietta
2003 Oxygen gradients in the microcirculation. Physiol Rev 83(3):933-63.

Van Assendelft, O. W.
1970 Spectrophotometry of Hemoglobin Derivatives. *In* Spectrophotometry of Haemoglobin Derivatives. O.W.V. Assendelft, ed. Pp. 47-73. Springfield, IL: C.C. Thomas.

Vandewalle, E., et al.
2013 Oximetry in glaucoma: correlation of metabolic change with structural and functional damage. Acta Ophthalmol.

Venkataraman, S. T., et al.
2008 Retinal arteriolar and capillary vascular reactivity in response to isoxic hypercapnia. Experimental eye research 87(6):535-542.

Vovenko, E.
1999 Distribution of oxygen tension on the surface of arterioles, capillaries and venules of brain cortex and in tissue in normoxia: an experimental study on rats. Pflügers Archiv : European journal of physiology 437(4):617-623.

Walshe, T. E., and P. A. D'Amore
2008 The role of hypoxia in vascular injury and repair. Annual Review of Pathology: Mechanisms of Disease 3(Journal Article):615-643.

Wanek, J., et al.
2011 Inner retinal metabolic rate of oxygen by oxygen tension and blood flow imaging in rat. Biomed Opt Express 2(9):2562-8.

Wanek, J., et al.

2013 Inner retinal oxygen delivery and metabolism under normoxia and hypoxia in rat. Invest Ophthalmol Vis Sci 54(7):5012-9.

Wang, L., and A. Bill
1997 Effects of constant and flickering light on retinal metabolism in rabbits. Acta Ophthalmol Scand 75(3):227-31.

Wangsa-Wirawan, N. D., and R. A. Linsenmeier
2003 Retinal oxygen: fundamental and clinical aspects. Archives of Ophthalmology 121(4):547-557.

Weidner, C.
1976 The c-wave in the ERG of albino rat. Vision Res 16(7):753-63.

Wilson, D. F., et al.
2005a Imaging oxygen pressure in the retina of the mouse eye. Adv Exp Med Biol 566:159-65.

Wilson, D. F., et al.
2005b Oxygen distribution and vascular injury in the mouse eye measured by phosphorescence-lifetime imaging. Applied Optics 44(25):5239-5248.

Wright, W. S., et al.
2012 Retinal blood flow abnormalities following six months of hyperglycemia in the Ins2(Akita) mouse. Exp Eye Res 98:9-15.

Yamauchi, H., et al.
1999 Significance of increased oxygen extraction fraction in five-year prognosis of major cerebral arterial occlusive diseases. J Nucl Med 40(12):1992-8.

Yi, J., et al.
2013 Visible-light optical coherence tomography for retinal oximetry. Opt Lett 38(11):1796-8.

Yoneya, S., et al.
2002 Retinal oxygen saturation levels in patients with central retinal vein occlusion. Ophthalmology 109(8):1521-1526.

Yu, D. Y., and S. J. Cringle
2001 Oxygen distribution and consumption within the retina in vascularised and avascular retinas and in animal models of retinal disease. Progress in retinal and eye research 20(2):175-208.

Yu, D. Y., et al.
1994 Intraretinal oxygen distribution in rats as a function of systemic blood pressure. Am J Physiol 267(6 Pt 2):H2498-507.

Yu, D. Y., et al.
2007 Intraretinal oxygen distribution and consumption during retinal artery occlusion and graded hyperoxic ventilation in the rat. Invest Ophthalmol Vis Sci 48(5):2290-6.

Zhou, Y., and A. W. Toga
1999 Efficient Skeletonization of Volumetric Objects. IEEE Transactions on Visualization and Computer Graphics 5(3):196-209.

Zijlstra, W. G., A. Buursma, and W. P. Meeuwsen-van der Roest
1991 Absorption spectra of human fetal and adult oxyhemoglobin, de-oxyhemoglobin, carboxyhemoglobin, and methemoglobin. Clin Chem 37(9):1633-8.

APPENDICES

APPENDIX A

License Agreement for Use of Fig 1

This is an Agreement between Pangyu Teng ("You") and Elsevier ("Elsevier"). It consists of your order details, the terms and conditions provided by Elsevier ("Elsevier"), and the payment terms and conditions.

Order Number	500867378
Order Date	May 01, 2014
Licensed content publisher	Elsevier
Licensed content publication	Elsevier Books
Licensed content title	Encyclopedia of the Eye
Licensed content author	B. Anand-Apte,J.G. Hollyfield
Licensed content date	2010
Number of pages	7
Start Page	9
End Page	15
Type of Use	reuse in a thesis/dissertation
Portion	figures/tables/illustrations
Number of figures/tables/illustrations	1
Format	electronic
Are you the author of this Elsevier chapter?	No
Will you be translating?	No
Title of your thesis/dissertation	Quantification of Retinal Oxygen Extraction Fraction and Vascular Oxygen Tension Gradients
Expected completion date	Jun 2014
Estimated size (number of pages)	
Elsevier VAT number	GB 494 6272 12
Permissions price	Not Available
VAT/Local Sales Tax	Not Available
Total	Not Available

APPENDIX B

License Agreement for Use of Text, Figures and Tables in Chapter V

This is a License Agreement between Pangyu Teng ("You") and Association for Research in Vision and Ophthalmology ("Association for Research in Vision and Ophthalmology") The license consists of your order details, the terms and conditions provided by Association for Research in Vision and Ophthalmology, and the payment terms and conditions.

License number	Reference confirmation email for license number
License date	May 01, 2014
Licensed content publisher	Association for Research in Vision and Ophthalmology
Licensed content title	Investigative ophthalmology
Licensed content date	Jan 1, 1977
Type of use	Thesis/Dissertation
Requestor type	Academic institution
Format	Electronic
Portion	chapter/article
Title or numeric reference of the portion(s)	Entire article of : Inner retinal oxygen extraction fraction in rat.
Title of the article or chapter the portion is from	Inner retinal oxygen extraction fraction in rat.
Editor of portion(s)	n/a
Author of portion(s)	Pang-yu Teng
Volume of serial or monograph	54
Issue, if republishing an article from a serial	1
Page range of portion	None
Publication date of portion	2013 Jan 21
Rights for	Main product
Duration of use	Life of current edition
Creation of copies for the disabled	no
With minor editing privileges	yes
For distribution to	United States
In the following language(s)	Original language of publication
With incidental promotional use	no

Lifetime unit quantity of new product	0 to 499
Made available in the following markets	university libraries
Specified additional information	Invest Ophthalmol Vis Sci. 2013 Jan 21;54(1):647-51. doi: 10.1167/iovs.12-11305.
The requesting person/organization	Pang-yu Teng
Order reference number	None
Author/Editor	Pang-yu Teng
The standard identifier	requested article is part of my own phd thesis
The proposed price	0
Title	Quantification of Retinal Oxygen Extraction Fraction and Vascular Oxygen Tension Gradients
Publisher	Univeresity of Illinois at Chicago
Expected publication date	Jun 2014
Estimated size (pages)	100
Billing Type	Invoice
Billing address	1905 W Taylor Street, LB103 CHICAGO, IL 60612 United States
Total (may include CCC user fee)	0.00 USD

APPENDIX C

License Agreement for Use of Text and Figures in Chapter VII

This is a License Agreement between Pangyu Teng ("You") and Springer ("Springer") provided by Copyright Clearance Center ("CCC"). The license consists of your order details, the terms and conditions provided by Springer, and the payment terms and conditions.

All payments must be made in full to CCC. For payment instructions, please see information listed at the bottom of this form.

License Number	3380430075718
License date	May 01, 2014
Order Content Publisher	Springer
Order Content Publication	Graefe's Archive for Clinical and Experimental Ophthalmology
Order Content Title	Oxygen tension and gradient measurements in the retinal microvasculature of rats
Order Content Author	Pang-yu Teng
Order Content Date	Jan 1, 2011
Volume number	250
Issue number	3
Type of Use	Thesis/Dissertation
Portion	Full text
Number of copies	1
Author of this Springer article	Yes and you are the sole author of the new work
Order reference number	None
Title of your thesis / dissertation	Quantification of Retinal Oxygen Extraction Fraction and Vascular Oxygen Tension Gradients
Expected completion date	Jun 2014
Estimated size(pages)	100
Total	**0.00 USD**

VITA

NAME: Pang-yu Teng

EDUCATION:

BS, Department of Biomedical Engineering, Chung Yuan Christian University, Chungli, Taiwan, 2005

MS, Department of Bioengineering, University of Illinois at Chicago, Chicago, Illinois, USA, 2009

PhD, Department of Bioengineering, University of Illinois at Chicago, Chicago, Illinois, USA, 2014

PROFESSIONAL MEMBERSHIP:

Association for Research in Vision and Ophthalmology

Institute of Electrical and Electronics Engineers

PUBLICATIONS:

· Teng P, Bagci AM, Alperin N , “Automated Prescription of an Optimal Imaging Plane for Measurement of Cerebral Blood Flow by Phase Contrast Magnetic Resonance Imaging ”, IEEE Trans Biomed Eng. 2011;58(9):2566-73.

· Wanek J, Teng P, Albers J, Blair NP, Shahidi M,"Inner Retinal Metabolic Rate of Oxygen by Oxygen Tension and Blood Flow Imaging in Rat", Biomed Opt Express. 2011;2(9):2562-8.

· Teng P, Blair NP, Wanek J, Shahidi M, "Oxygen Tension and Gradient Measurements in the Retinal Microvasculature of Rats", Graefes Arch Clin Exp Ophthalmol. 2012;250(3):361-7.

· Gaynes B, Teng P, Wanek J, Shahidi M, "Feasibility of Conjunctival Hemodynamic Measurements in Rabbits: Reproducibility, Validity and Response to Acute Hypotension", Microcirculation. 2012;19(6):521-9.

· Teng P, Wanek J, Blair NP, Shahidi M, "Inner Retinal Oxygen Extraction Fraction in Rat", Invest Ophth Vis Sci. 2013; 54(1):647-51.

· Wanek J, Teng P, Blair NP, Shahidi M,"Inner Retinal Oxygen Delivery and Metabolism Under Normoxia and Hypoxia in Rat", Invest Ophth Vis Sci. 2013; 54(7):5012-9.

· Mezu-Ndubuisi OJ, Teng P, Wanek J, Blair NP, Chau FY, Reddy NM, Raj JU, Reddy SP, Shahidi M, "In-vivo Retinal Vascular Oxygen Tension Imaging and Fluorescein Angiography in the Mouse Model of Oxygen-Induced Retinopathy", Invest Ophth Vis Sci. 2013; 54(10):6968-72.

· Wanek J, Teng P, Blair NP, Shahidi M, "Inner Retinal Oxygen Delivery and Metabolism in Streptozotocin Diabetic Rats", Invest Ophth Vis Sci. 2014; accepted.

· Mezu-Ndubuisi OJ, Wanek J, Chau FY, Teng P, Blair NP, Reddy NM, J Raj U, Reddy SP, Shahidi M, "Correspondence of Retinal Thinning and Vasculopathy in Mice with Oxygen-Induced Retinopathy", Exp Eye Res. 2014; accepted.

ABSTRACTS:

· Teng P, Li A, Lin S, Su J, Weng C, “Analysis of the Correlation between Facial Temperature and the Stenosis of Carotid Arteries”, Conf. Proc. IEEE Eng. Med. Biol. Soc., 6277-6280 (2006)

· Wanek J, Teng P, Blair NP, Shahidi M, "A New Imaging Method for Assessment of Inner Retinal Oxygen Consumption in Rat", presented at ARVO meeting, Ft Lauderdale, FL (2011)

· Teng P, Blair NP, Wanek J, Yildirim I, Shahidi M, "Longitudinal Gradients of Oxygen Tension in the Retinal Vasculature of Rat", presented at ARVO meeting, Ft Lauderdale, FL (2011)

· Gaynes BI, Teng P, Wanek J, Shahidi M, "Hemorheologic and Hemodynamic Response of Conjunctival Microcirculation to Acute Hypotension in Rabbits", presented at ARVO meeting, Ft Lauderdale, FL (2012)

· Chau FY , Mezu-Ndubuisi OJ, Reddy NM, Wanek J, Teng P, Blair NP, Reddy SP, Shahidi M, "Spectral Domain Optical Coherence Tomography (SDOCT) Findings in a Mouse Model of Retinopathy of Prematurity", presented at ARVO meeting, Ft Lauderdale, FL (2012)

· Mezu-Ndubuisi OJ, Wanek J, Teng P, Chau FY, Reddy NM, Lin A, Blair NP, Reddy SP, Shahidi M, "Retinal Vascular Oxygen Tension Imaging and Fluorescein Angiography in a Mouse Model of Retinopathy of Prematurity", presented at ARVO meeting, Ft Lauderdale, FL (2012)

· Wanek J, Teng P, Norman NP, Shahidi M, "Global Inner Retinal Metabolic Rate of Oxygen During Hypoxia in Rat", presented at ARVO meeting, Ft Lauderdale, FL (2012)

· Teng P, Wanek J, Norman NP, Shahidi M, "Retinal Oxygen Extraction Fraction: the Ratio of Oxygen Consumption to Delivery", presented at ARVO meeting, Ft Lauderdale, FL (2012)

· Wanek J, Teng P, Norman NP, Shahidi M, "Inner Retinal Oxygen Metabolism and Delivery in Streptozotocin Diabetic Rats", presented at ARVO meeting, Seattle, WA (2013)

· Teng P, Wanek J, Norman NP, Shahidi M, "Response of Inner Retinal Oxygen Extraction Fraction to Light Flicker in Rat", presented at ARVO meeting, Seattle, WA (2013)

· Chau FY, Mezu-Ndubuisi OJ, Wanek J, Teng P, Blair NP, Zelkha R, Reddy NM, Reddy SP, Shahidi M, "Alterations in Thickness of Retinal Layers in a Mouse Model of Retinopathy of Prematurity by Spectral Domain Optical Coherence Tomography", presented at ARVO meeting, Orlando, FL (2014)

· Wanek J, Teng P, Norman NP, Shahidi M, "Inner Retinal Oxygen Metabolism and Delivery in Streptozotocin Diabetic Rats", presented at ARVO meeting, Orlando, FL (2014)

· Teng P, Wanek J, Norman NP, Shahidi M, "A Method for Three-dimensional Mapping of Retinal Tissue Oxygen Tension in Rat", presented at ARVO meeting, Orlando, FL (2014)